

**Synthesis of ZnO-NiO nanoparticle using  
solid-vapor phase thermal sublimation method**

by

**Ahmad Shuhadah Bin Ismail**

Dissertation submitted in partial fulfilment of  
the requirements for the  
Bachelor of Engineering (Hons)  
(Chemical Engineering)

JULY 2009

Universiti Teknologi PETRONAS  
Bandar Seri Iskandar  
31750 Tronoh  
Perak Darul Ridzuan

CERTIFICATION OF APPROVAL

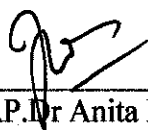
**Synthesis of ZnO-NiO nanoparticle using solid–vapor phase  
thermal sublimation method**

by

Ahmad Shuhadah Bin Ismail

A project dissertation submitted to the  
Chemical Engineering Programme  
Universiti Teknologi PETRONAS  
in partial fulfilment of the requirement for the  
BACHELOR OF ENGINEERING (Hons)  
(CHEMICAL ENGINEERING)

Approved by,



(AP. Dr Anita Ramli)

**DR ANITA RAMLI**  
Associate Professor  
Fundamental & Applied Sciences Department  
Universiti Teknologi PETRONAS, PERAK

UNIVERSITI TEKNOLOGI PETRONAS

TRONOH, PERAK

July 2009

## ABSTRACT

This report basically discusses the preliminary research done and basic understanding of the chosen topic, which is the “Synthesis of ZnO-NiO nanoparticle using solid–vapor phase thermal sublimation method”. This project will apply solid–vapor phase thermal sublimation method to synthesis ZnO-NiO nanoparticle, to study and characterize the effect of different ratios of ZnO-NiO used in determining its physico-chemical properties, study and characterize the effect of different calcinations temperatures of ZnO-NiO used in determining its physico-chemical properties, and to study the effect of introducing NiO to ZnO towards the electrical properties of zinc oxide. For this study, ZnO and NiO is prepared via solid–vapor phase thermal sublimation method. The chemicals used are Zinc Chloride and Nickel(ii)Nitrate which will be mixed with distilled water and it will undergo heating and stirring process on a hot plate. The ratio of Zinc Chloride with Nickel (ii) Nitrate will be varied to study the effect of using different concentrations of mixed solution. Then the mixed solution will undergo reflux process and will be put in an oven for drying process. The dried solution will be transferred in a furnace for solid–vapor phase thermal sublimation process to produce ZnO-NiO nanoparticle. The furnace temperatures will be varied to study the relation of heat treatment with formation of catalyst. The textural and morphological of the nanoparticle will be tested with XRD, SEM and Uv-Vis will be conducted to study the nanoparticle’s electrical properties.

## **ACKNOWLEDGEMENT**

First of all I want to thank to the God for his blessing. Finally I manage to complete my final year project without any delay. I also want to thank my supervisor Ap.Dr. Anita Ramli for his guidance and knowledge. Without him this project will not be successful. Not forgetting my beloved friends that have supported me during experimental works. To the Universiti Teknologi PETRONAS (UTP) staffs, I feel grateful because they have provided me with such fantastic facilities that have helped me undergoing the experiment. I hope from this project, it will benefit the industries and help to improve the nanomaterials industry and knowledge.

## TABLE OF CONTENTS

<b>CERTIFICATION OF APPROVAL</b> .....	<b>i</b>
<b>CERTIFICATION OF ORIGINALITY</b> .....	<b>ii</b>
<b>ABSTRACT</b> .....	<b>iii</b>
<b>ACKNOWLEDGEMENT</b> .....	<b>iv</b>
<b>CHAPTER 1:</b>	
<b>INTRODUCTION</b> .....	<b>1</b>
1.1 Background of Study.....	1
1.2 Problem Statement.....	2
1.3 Objectives & Scope of Study.....	3
<b>CHAPTER 2: LITERATURE</b>	
<b>REVIEW</b> .....	<b>4</b>
2.1 About Zinc Oxide.....	4
2.2 Application of zinc oxide.....	7
2.3 Effect of Calcination Temperature on the Properties of Mixture....	9
2.4 ZnO nanoparticles, ZnO Band Gap and Electrical Resistivity.....	15
2.5 Effect of Different Ratios of Mixture Used.....	19
2.6 About NiO.....	24
2.7 Properties of Nickel Oxide.....	25
2.8 Reflux.....	36
<b>CHAPTER 3:</b>	
<b>METHODOLOGY</b> .....	<b>33</b>
3.1 Research Methodology.....	33
3.2 Project Activities.....	33
3.3 Chemicals List.....	34
3.4 Equipment List.....	34
3.5 Experiment Procedures.....	36
3.6 Project Process Flow (Gantt Chart).....	38

<b>CHAPTER 4: RESULT AND</b>	
<b>DISCUSSION.....</b>	<b>39</b>
4.1 Results.....	39
4.2 UV-Vis Results.....	44
4.3 Discussion.....	50
<b>CHAPTER 5: CONCLUSION AND</b>	
<b>RECOMMENDATION.....</b>	<b>52</b>
<b>REFERENCES.....</b>	<b>53</b>

## **LIST OF FIGURES**

- Fig 2.1** : Wurtzite structure.
- Fig 2.2** : Zincblende unit cell
- Fig 2.3** : Synthetic ZnO Crystals. Red and green color are associated with different concentrations of oxygen vacancies
- Fig 2.4** : TG/DTA curves of ZnO previously dried at 110oC, (a) controlled and (b) freeze drying
- Fig 2.5** : X-ray diffraction patterns of o = ZnO, x = NaNO<sub>3</sub> and v = ZnCO<sub>3</sub> powders treated at different temperatures a) prepared by controlled drying (S1) and b) prepared by freeze drying (S2).
- Fig 2.6** : Infrared spectra of ZnO powders treated at different temperatures a) prepared by controlled drying (S1) and b) prepared by freeze drying (S2).
- Fig 2.7** : Images of ZnO powders treated at different temperatures a) S1 - 100oC, b) S1 - 800oC, c) S2 - 100oC and d) S2 - 800oC
- Fig 2.8** : Adsorption-desorption isotherms of ZnO nanoparticles (S1) treated at different temperatures: (a) 110oC, (b) 200oC, (c) 400oC, (d) 600oC, (e) 800oC and f) 1000oC
- Fig 2.9.** : (a) Room temperature optical absorption spectrum of the ZnO nanowires. (b) Room temperature PL spectra of the ZnO nanonails and nanowire arrays.
- Fig 2.10.** : Log resistance versus inverse temperature plot for the ZnO nanonail array
- Fig 2.11.** : Change of dc resistance of the ZnO nanonail array as a function of time in different gases at different concentrations and temperatures: (a) 200 ppm of CO at 225 °C, (b) 200 ppm of NO<sub>2</sub> at 225 °C, and (c) 100 ppm of H<sub>2</sub>S at 100 °C.
- Fig 2.12** : XRD patterns of ZIO films for different In:Zn ratios.
- Fig 2.13** : Cross sectional TEM images of ZIO channel layers with Zn/(In + Zn) of a) 70 at% and b) 60 at%.

- Fig 2.14** : Compositional dependence of film resistivity. The numbers indicated in the legend denote the passing time in hours after the deposition of the film
- Fig 2.15** : Effect of duration on ZIO-TFTs performances. a) Compositional dependence of  $V_{th}$  shift. Here,  $|\Delta V_{th}|$
- Fig 2.16** : Nickel Oxide Structure
- Fig. 2.17.** : Scanning electron microscopic (SEM) image of NiO nanoparticles
- Fig. 2.18.** : Transmission electron microscopic (TEM) images of NiO Nanoparticle (a) lower magnification and (b) higher magnification (inset in (a) showed the selected area electron diffraction pattern).
- Fig. 2.19.** : XRD pattern of NiO nanoparticles
- Fig. 2.20.** : Raman spectrum of NiO nanoparticles.
- Fig. 2.21** : UV–visible absorption spectrum of NiO nanoparticles.
- Fig. 2.22.** : FT-IR spectra: (a) nickel acetate/PVAc precursor and (b) NiO nanoparticles.
- Fig 2.23** : Reflux Set
- Fig 2.24** : Common reflux preparation
- Fig 3.25** : Hot plate
- Fig 3.26** : Reflux Set-up
- Fig 3.27** : Vacuum Filter
- Fig 4.28** : Sample after reflux process ( more concentrated than before)
- Fig 4.29** : Sample after filtration
- Fig 4.30** : Sample after being treated in the furnace
- Fig 4.31** : Samples in three different calcinations temperatures
- Fig 4.32** : Sample after reflux process
- Fig 4.33** : Sample after filtration
- Fig 4.34** : Sample after being treated in the furnace
- Fig 4.35** : Samples in 3 different calcinations temperature
- Fig 4.36** : Solution after being refluxed



- Fig 4.37** : Solution after being filtration
- Fig 4.38** : Samples after being treated in the furnace
- Fig 4.39** : Sample in three different calcinations temperatures
- Fig 4.40** : Zinc Chloride
- Fig 4.41** : Sample at different calcinations temperatures
- Fig 4.42** :0.2 mol zinc chloride with 0.2 mol nickel(ii)nitrate (400 °C)
- Fig 4.43** :0.2 mol zinc chloride with 0.2 mol nickel(ii)nitrate (500 °C)
- Fig 4.44** :0.2 mol zinc chloride with 0.2 mol nickel(ii)nitrate (600 °C)
- Fig 4.45** :0.5 mol zinc chloride with 0.2 mol nickel(ii)nitrate (400 °C)
- Fig 4.46** :0.5 mol zinc chloride with 0.2 mol nickel(ii)nitrate (500 °C)
- Fig 4.47** :0.5 mol zinc chloride with 0.2 mol nickel(ii)nitrate (600 °C)
- Fig 4.48** :0.7 mol zinc chloride with 0.2 mol nickel(ii)nitrate (400 °C)
- Fig 4.49** :0.7 mol zinc chloride with 0.2 mol nickel(ii)nitrate (500 °C)
- Fig 4.50** :0.7 mol zinc chloride with 0.2 mol nickel(ii)nitrate (600 °C)
- Fig 4.51** :Approximately 0.5 mol of Zinc Chloride (400 °C)
- Fig 4.52** :Approximately 0.5 mol of Zinc Chloride (500 °C)
- Fig 4.53** :Approximately 0.5 mol of Zinc Chloride (600 °C)

## **LIST OF TABLES**

**Table 2.1** : Textural and morphological characteristics of the ZnO

**Table 3.2** : Gantt Chart for FYP II

# CHAPTER 1

## INTRODUCTION

### 1.1 Background of Study

In materials science, ZnO is often called a II-VI semiconductor because zinc and oxygen belong to the 2nd and 6th groups of the periodic table, respectively. This semiconductor has several favorable properties: good transparency, high electron mobility, wide bandgap, strong room-temperature luminescence, etc. Those properties are already used in emerging applications for transparent electrodes in liquid crystal displays and in energy-saving or heat-protecting windows and electronic applications of ZnO as thin-film transistor and light - emitting diode are forthcoming as of 2009. NiO can be prepared by multiple methods. Upon heating above 400 °C, nickel powder reacts with oxygen to give NiO. In some commercial processes, green nickel oxide is made by heating a mixture of nickel powder and water at 1000 °C, the rate for this reaction can be increased by the addition of NiO [3]. The simplest and most successful method of preparation is through pyrolysis of a nickel (II) compounds such as th hydroxide, nitrate, and carbonate, which yield a light green powder [4]. Synthesis from the elements by heating the metal in oxygen can yield grey to black powders which indicates nonstoichiometry [4]. The Reflux Mode used for the highest degree of purifications is generally selected for the distillation of vodka, neutral spirits, and water, where extremely high purity is desired. When distilling in reflux mode, it is extremely advantageous to have a longer column than in traditional distillation. In addition, filling is added to the column for the refluxing liquid to flow down through, aiding in increased purity. There are many forms of column packing available, varying in surface area and material.

## 1.2 Problem Statement

By the year 2014, the market revenue for nanotechnology-related products is expected to reach 2.6 trillion US dollars (USD) [5]. From a survey funded by the European Commission (2006) [6], four interesting observations are discovered as follows. Firstly, 74% of enterprises working on nanomaterials are small and medium scale enterprises (SMEs). The second finding is that the most important success factors are superior material properties (78%), quality improvement (47%), cooperation with other companies (37%) and collaboration with research organisations (33%). Thirdly, the most important obstacles for the application of nanomaterials by SMEs are problems with production process technology (41%), high production costs (37%), lack of knowledge transfer from scientific communities to SMEs (33%) and small market volume (18%). Finally, 68% of the 190 respondents spend only 10% of their research investment for external research projects - this data implies that most companies carry out research activities on their own. Superior materials properties is the major motivation, imperfect manufacturing technology causes high production costs, and poor university industry collaboration is noted [3]. As a result, the cost of nanomaterials becomes too high for potential manufacturers to use them in their products. Therefore, most of the industrial nano-research activities focus on making their nano-products cheap enough in order to be competitive. nanotechnology is still at its infancy when it comes to real application. One of the main reasons is the high cost of nanomaterials, as mentioned earlier, that can be hundreds of US dollars per kg or even thousands of US dollar per kg for specialty nanomaterials [1]. The relax method and solid–vapor phase thermal sublimation method is chosen since it requires low costs of money and also not too complicated and sloppy process. Some of the other methods suffer from the difficulty in size-homogeneity and well dispersion of nanoparticles and also such processes require catalysts that will unavoidably influence the purity of the ZnO-NiO nanofoms and they could have an effect on the physical properties of these products [46].

## **1.2 Objectives & Scope of Study**

The objective of the project is to

- i) apply reflux method to synthesis NiO-ZnO nanoparticle
- ii) study and characterize the effect of different ratios of ZnO-NiO used in determining its physico-chemical properties
- iii) study and characterize the effect of different calcinations temperatures of ZnO-NiO used in determining its physico-chemical properties
- iv) study the effect of introducing NiO to ZnO towards the electrical properties of zinc oxide.

The scope of work for this project is to conduct and study the synthesis of NiO-ZnO nanoparticle using reflux method. The chemicals that will be used are zinc chloride and nickel(ii) nitrate

## CHAPTER 2

### LITERATURE REVIEW

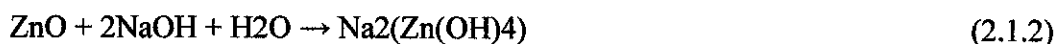
#### 2.1 About Zinc Oxide

Zinc oxide is an inorganic compound with the formula ZnO. It usually appears as a white powder, nearly insoluble in water. The powder is widely used as an additive into numerous materials and products including plastics, ceramics, glass, cement, rubber (e.g. car tyres), lubricants,[8] paints, ointments, adhesives, sealants, pigments, foods (source of Zn nutrient), batteries, ferrites, fire retardants, first aid tapes, etc. ZnO is present in the Earth crust as a mineral zincite; however, most ZnO used commercially is produced synthetically. In materials science, ZnO is often called a II-VI semiconductor because zinc and oxygen belong to the 2nd and 6th groups of the periodic table, respectively. This semiconductor has several favorable properties: good transparency, high electron mobility, wide bandgap, strong room-temperature luminescence, etc. Those properties are already used in emerging applications for transparent electrodes in liquid crystal displays and in energy-saving or heat-protecting windows, and electronic applications of ZnO as thin-film transistor and light-emitting diode are forthcoming as of 2009.

Zinc oxide is an amphoteric oxide. It is nearly insoluble in water and alcohol, but it is soluble in (degraded by) most acids, such as hydrochloric acid:[11][12]



Bases also degrade the solid to give soluble zincates:



ZnO reacts slowly with fatty acids in oils to produce the corresponding carboxylates, such as oleate or stearate. ZnO forms cement-like products when mixed with a strong aqueous solution of zinc chloride and these are best described as zinc hydroxy

chlorides.[13] This cement was used in dentistry.[14] ZnO also forms cement-like products when treated with phosphoric acid; related materials are used in dentistry.

ZnO decomposes into zinc vapor and oxygen only at around 1975 °C, reflecting its considerable stability. Heating with carbon converts the oxide into the metal, which is more volatile than the oxide.[16]



Zinc oxide can react violently with aluminum and magnesium powders, with chlorinated rubber and linseed oil on heating causing fire and explosion hazard.[17][18]

It reacts with hydrogen sulfide to give the sulfide: this reaction is used commercially in removing H<sub>2</sub>S using ZnO powder (e.g., as deodorant).



When ointments containing ZnO and water are melted and exposed to ultraviolet light, hydrogen peroxide is produced.[12]

Zinc oxide crystallizes in three forms: hexagonal wurtzite, cubic zincblende, and the rarely observed cubic rocksalt). The wurtzite structure is most stable at ambient conditions and thus most common . The zincblende form can be stabilized by growing ZnO on substrates with cubic lattice structure. In both cases, the zinc and oxide centers are tetrahedral. The rocksalt (NaCl-type) structure is only observed at relatively high pressures about 10 GPa.[19].Hexagonal and zincblende polymorphs have no inversion symmetry (reflection of a crystal relatively any given point does not transform it into itself). This and other lattice symmetry properties result in piezoelectricity of the hexagonal and zincblende ZnO, and in pyroelectricity of hexagonal ZnO.The hexagonal structure has a point group 6 mm (Hermann-Mauguin

notation) or  $C6v$  (Schoenflies notation), and the space group is  $P63mc$  or  $C6v4$ . [19] As in most II-VI materials, the bonding in ZnO is largely ionic, which explains its strong piezoelectricity. Due to the polar Zn-O bonds, zinc and oxygen planes bear electric charge (positive and negative, respectively). Therefore, to maintain electrical neutrality, those planes reconstruct at atomic level in most relative materials, but not in ZnO - its surfaces are atomically flat, stable and exhibit no reconstruction. This anomaly of ZnO is not fully explained yet. [15]

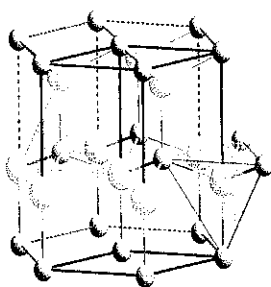


**Figure 2.1** : Wurtzite structure.

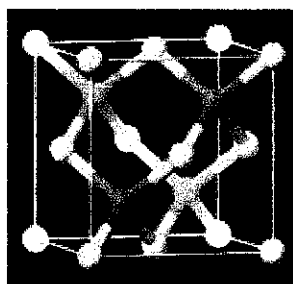


**Figure 2.2** : Zincblende unit cell

ZnO is a relatively soft material with approximate hardness of 4.5 on the Mohs scale. [13] Its elastic constants are smaller than those of relevant III-V semiconductors, such as GaN. The high heat capacity and heat conductivity, low thermal expansion and high melting temperature of ZnO are beneficial for ceramics. [20] Among the tetrahedrally bonded semiconductors, it has been stated that ZnO has the highest piezoelectric tensor or at least one comparable to that of GaN and AlN. [21] This property makes it a technologically important material for many piezoelectrical applications, which require a large electromechanical coupling.

ZnO has a relatively large direct band gap of  $\sim 3.3$  eV at room temperature, [19] therefore, pure ZnO is colorless and transparent. Advantages associated with a large band gap include higher breakdown voltages, ability to sustain large electric fields, lower electronic noise, and high-temperature and high-power operation. The bandgap of ZnO can further be tuned from  $\sim 3-4$  eV by its alloying with magnesium oxide or cadmium oxide. [19]. Most ZnO has n-type character, even in the absence of

intentional doping.[23] Controllable n-type doping is easily achieved by substituting Zn with group-III elements such as Al, Ga, In or by substituting oxygen with group-VII elements chlorine or iodine.[24].[19].Electron mobility of ZnO strongly varies with temperature and has a maximum of  $\sim 2000 \text{ cm}^2/(\text{V}\cdot\text{s})$  at  $\sim 80 \text{ K}$ .[20] Data on hole mobility are scarce with values in the range  $5\text{-}30 \text{ cm}^2/(\text{V}\cdot\text{s})$

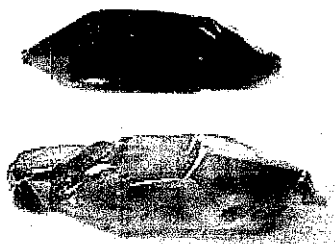


**Figure 2.3 :** Synthetic ZnO Crystals. Red and green color are associated with different concentrations of oxygen vacancies.[30]

## 2.2 Application of Zinc Oxide

Zinc oxide (ZnO) has attracted huge research effort due its potential versatile applications in ultraviolet (UV) photodetectors, chemical sensors, transparent electronics, spintronics, UV light emitters, surface acoustic devices, piezoelectric transducers, mechanical resonators, short-wavelength electronics, field effect transistors, logic gates, optical memory, light emission diodes, photovoltaic devices, superconductors, UV polymer nanocomposites, bacteria DNA detection, neuro networks, hydrogen fuel engine system, engine oil tribology, water treatment and rubber nano-accelerators [44]. The current applications of nano ZnO are very few in that the biggest users of nano ZnO are the sunscreen, cosmetics and pharmaceuticals industries, accounting for over 20000 metric ton (MT) in term of yearly consumption . Normally nano ZnO serves as an additive to sunscreen skin lotion, antiseptic soap/cream, antiseptic plaster, deodorant, anti-rash talc/cream, lipstick and facial cosmetics. The salient properties of nano ZnO that make it suitable for these healthcare products are anti-UVA, anti-UVB, antiseptic, antimicrobial, deodorant,



transparency, photo-stability, anti-aging, anti-fungus and anti-rash. Eventhough there has been a global concern on skin penetration of ZnO nanoparticles, work done by Cross et al, Gamer et al, Lademann et al, and Nohynek et al, have proven that nano ZnO (20-30 nm) is safe for human external usage whereby the penetration is very small (1.5-2.3%) and limited to the epidermis (dead skin cells). In fact, they found that nano ZnO is much safer than organic-base sunscreen agents that penetrate deeply into the flesh and organic agents are suspected to cause cancer. These recent findings would certainly promote research on nano ZnO since it is now proven that ZnO nanoparticles are biosafe, biocompatible and do not pose a real threat to researchers or workers as long as the powder is not inhaled. It is also worthy to note one of the earliest applications (in the 1970's) of nano ZnO is its function as the semiconductive-photoconductive agent for photocopy papers. Coloring dyes are absorbed on the large surfaces of ZnO that converts invisible short-wavelength light and long-wavelength infrared into visible light. Recent industrial work on nano ZnO has paved way for initial applications in nano-textiles whereby ZnO nanoparticles are embedded in polymer fabrics in order to introduce intriguing functions especially anti-UV, water repellent, antiseptic, deodorant, self-cleaning, wrinkle-free, fire-retardant, strength enhancing and anti-microbial. These novel textiles seem to produce wonder shirts and wonder jeans; however, the main obstacle still lies in the high cost of nano ZnO that exceeds USD 30/kg that makes nano-textiles too expensive for common public use. Despite progress in nano ZnO applications, micron-sized ZnO (micron ZnO) is still the dominant type that rules the global versatile applications that include rubber tyres, rubber products, ceramics, varistors, ferrites, paints, coatings, electronic glasses, fungistatic plastic packages, cements, anti-fouling marine coatings, livestock feed additives, cigarette filters, gas/fluid filters, and soil fertilizers. Zinc oxide is used in these products due to its unique benefits such as anti-UV, anti-aging, strength reinforcement, white pigmentation, sintering fluxing, anti-microbial, antiseptic, flame retardant, water repellent, self-cleaning, anti-fungus, anti-fouling, anti-algae, HCN-H<sub>2</sub>S filtering, animal growth stabilizing, plant growth regulator, ferrimagnetism, semiconducting and high-power energy handling. These highly versatile applications

of zinc oxide might explain why zinc is the fourth largest metal being mined in the world after iron, aluminium and copper.

### **2.3 Effect of Calcination Temperature on the Properties of Mixture**

Zinc nitrate and sodium carbonate were used as precursors of the ZnO particles. In a typical synthesis,  $\text{Zn}(\text{NO}_3)_2 \cdot 6\text{H}_2\text{O}$  were dissolved in deionized water in the molar ratio of 1:5, and mixed for homogenization during 1 h.  $\text{Na}_2\text{CO}_3$  were also dissolved in deionized water in the molar ratio of 7:10, and mixing with the zinc solution leading to the formation of a white precipitate. The precipitate was washed with deionized water to remove impurities. The obtained powder was separated in two aliquots to be submitted to drying processes. One aliquot (S1) was dried in an oven at  $110^\circ\text{C}$  for 48 h and the other (S2) was immersed in liquid nitrogen to freezing and then was lyophilized by 78 h at  $-40^\circ\text{C}$  and vacuum of 0.7 Pa. Both the aliquots were calcined at different temperatures between 200 and  $1000^\circ\text{C}$  for 2 hours. TG curve for the S1 sample (Fig:2.4a) shows three stages of weigh loss accompanied by two endothermic and two exothermic peaks in DTA curve. The first endothermic event between 100 and  $200^\circ\text{C}$  can be associated to removal of surface water of the sample with weight loss of 18%. The weight lost of 2% in the range of  $210\text{-}380^\circ\text{C}$ , accompanied by one endothermic and one exothermic peak, and of 2 % in the range of  $410\text{-}800^\circ\text{C}$  is due to the nitrate and  $\text{CO}_3$  decomposition. The broad and intense exothermic peak could be associated with the formation of the pure ZnO phase. The obtained residue is around 78% (pure ZnO phase).[45]

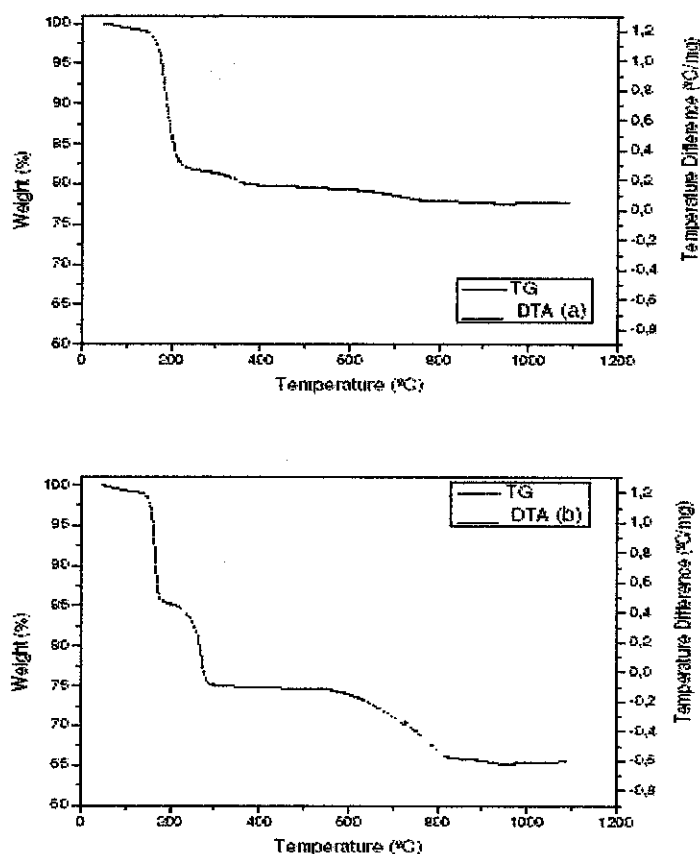
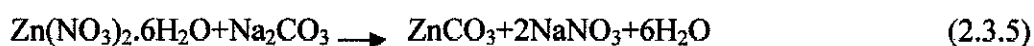
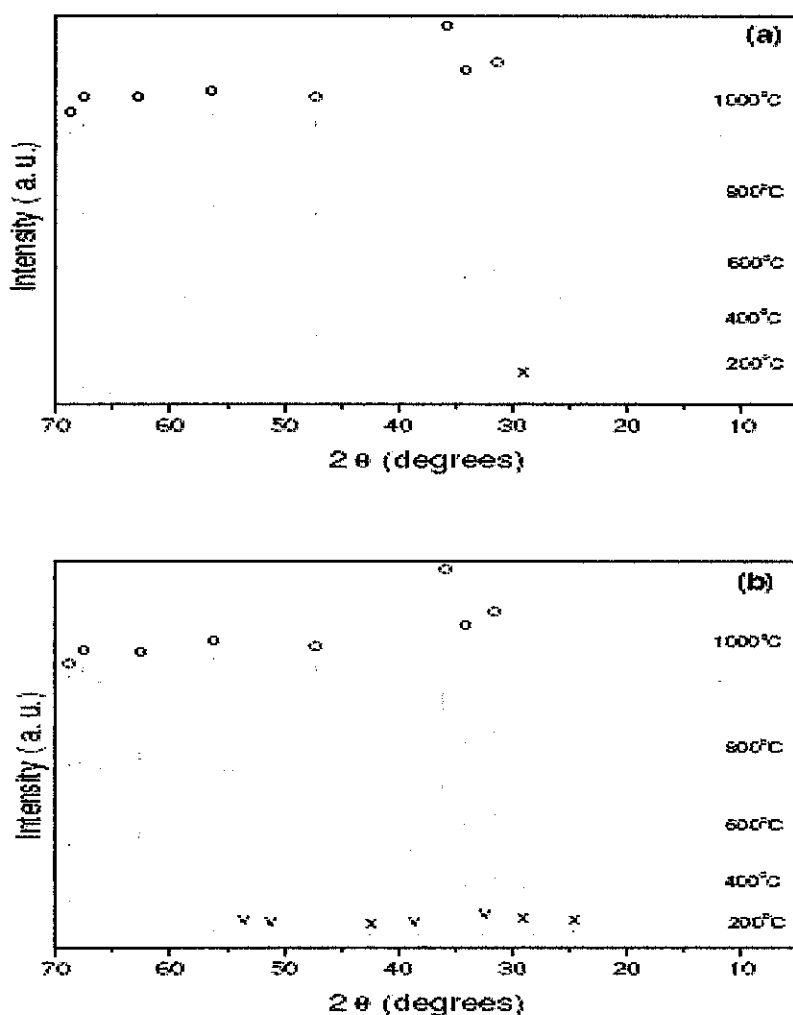


**Fig 2.4:** TG/DTA curves of ZnO previously dried at 110°C, (a) controlled and (b) freeze drying.

The S2 sample (Fig2.4b) lost 14% weight in the range of 50-180°C due to surface water removal related to an endothermic event. The other two endothermic events between 180-250°C and 580-820°C were attributed to loss of sodium nitrate (11%) and carbon dioxide (10 %). These events are accompanied by endothermic peaks in DTA curves. A broad exothermic event appears between 800 and 930°C, probably due to the formation of the pure ZnO phase. In this case, the residue obtained is around 65 %. We can describe the ZnO formation with the reaction below:

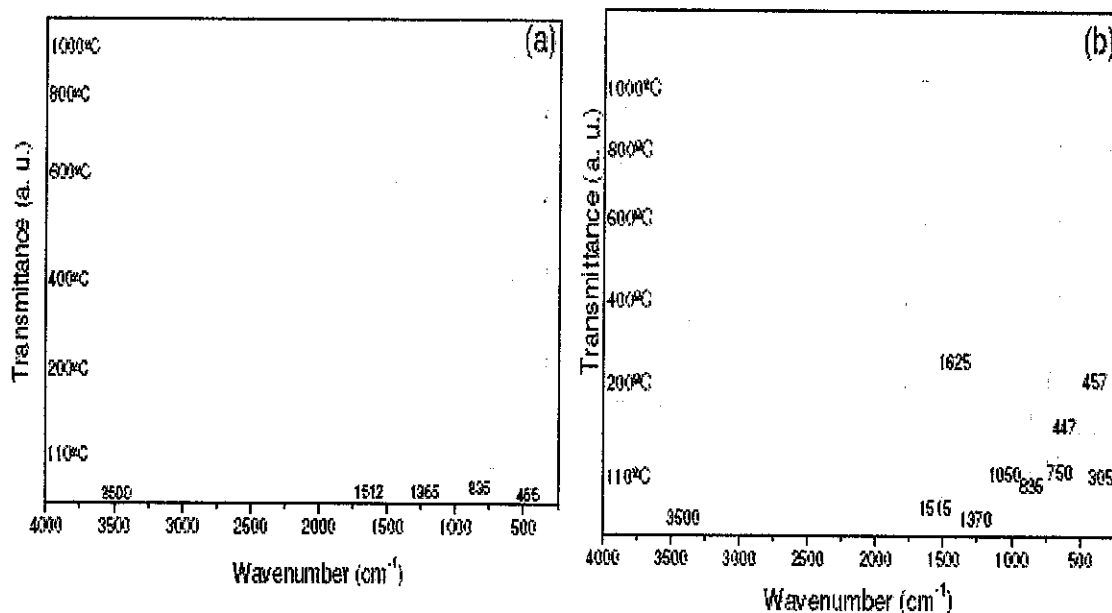


Figures 2.5a and 2.5b show XRD patterns of S1 and S2 samples calcined at various temperatures. The characteristic peaks of the ZnO phase increase in intensity above 200°C with the calcination temperature. The S1 sample presented peaks characteristics of ZnO phase at 200°C and by-products such as NaNO<sub>3</sub> and ZnCO<sub>3</sub>(4%), which decomposed gradually with increasing in the temperature. The pure phase of ZnO was formed below 800°C. The S2 sample shows peaks of ZnO phase with 21% of byproducts such as ZnCO<sub>3</sub> and NaNO<sub>3</sub> between 200 and 600°C, which decomposed with the increase in the temperature, originating pure phase of ZnO above 800°C.



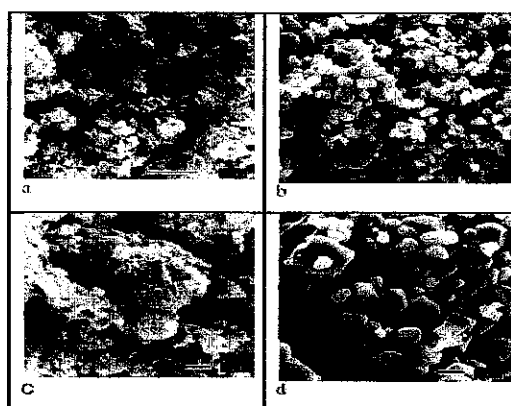
**Fig 2.5:** X-ray diffraction patterns of o = ZnO, x = NaNO<sub>3</sub> and v = ZnCO<sub>3</sub> powders treated at different temperatures a) prepared by controlled drying (S1) and b) prepared by freeze drying (S2).

Figure 2.6 shows infrared spectra of the ZnO samples (S1 and S2) treated at various temperatures. The spectra show bands ( $3500\text{ cm}^{-1}$ ) assigned to OH stretching vibrations of crystalline and adsorbed H<sub>2</sub>O. Two bands were observed at 1512 and  $1365\text{ cm}^{-1}$ , corresponding to n3 frequency of carbonate groups (C – O and C = O). In the spectra of S1 sample, these bands disappear after treatment at 600°C and in S2 spectra only after 800°C. Bands at  $1050\text{ cm}^{-1}$ ,  $835\text{ cm}^{-1}$  and  $703\text{ cm}^{-1}$  relate to  $\nu_1$ ,  $\nu_2$ ; and  $\nu_4$  frequencies of the carbonate appear in S1 spectra only for treatment at 110°C and in S2 spectra until treatment at 800°C. Bands with small intensity characteristics of nitrate groups appear at  $1630\text{ cm}^{-1}$ . These bands disappear only above heating at 800°C. The S1 spectra show a broad band between 550 and  $465\text{ cm}^{-1}$  with shoulder shape, characteristic of hexagonal Zn-O phase. With the increasing in the calcination temperature, the shoulder shape changes and a unique broad band is formed. The S2 spectra also show a broad band, without the shoulder shape, more intense than the S1 sample ones. The shape of the IR bands can be due to the geometry and size of the particles, and/or the aggregate formation.



**Fig 2.6:** Infrared spectra of ZnO powders treated at different temperatures a) prepared by controlled drying (S1) and b) prepared by freeze drying (S2).

The IR spectra show that the S2 sample has more impurities than the S1 sample, according to XRD patterns and TG/DTA curves, confirming the difference between the powders produced in both the process. Figure 2.7 shows the morphology of the ZnO. The images obtained by SEM of the S1 samples treated at 110°C (Fig.2.7a) show plate-like nanoparticles forming agglomerates. After treatment at 800°C, these particles (Fig:2.7b) grow and densify, reaching an average particle size of  $0.550 \pm 0.050 \mu\text{m}$ . The S2 images (Fig. 2.7c) also shows plate-like nanoparticles, which grow after treatment at 800°C (Fig:2.7d), reaching an average particle size of  $1.1 \pm 0.1 \mu\text{m}$ . The samples showed significant morphological differences. Table 2.1 shows the textural characteristics of ZnO samples treated at various temperatures. S1 samples had specific surface area, porosity and true density larger than S2 samples. We also can observe that the average particle size measured by BET method is according to the results obtained by SEM.



**Fig 2.7:** Images of ZnO powders treated at different temperatures a) S1 - 100°C, b) S1 - 800°C, c) S2 - 100°C and d) S2 - 800°C.

Temperature (°C)	SSA ( $\text{m}^2 \text{g}^{-1}$ )	True Density ( $\text{g.cm}^{-3}$ )	Total pore volume ( $10^{-3} \text{cm}^3 \text{g}^{-1}$ )	Average particle size (nm)	Average crystallite size by XRD (nm)
<i>Controlled drying</i>					
110	59.1	3.5	48	40	12
200	27.2	3.9	55	57	29
400	17.1	4.2	23	84	35
600	7.2	4.5	10	135	45
800	2.1	4.8	2	595	64
<i>Freeze drying</i>					
<i>As-prepared</i>					
200	7.2	3.0	8	278	35
400	2.0	2.3	1	909	66
600	1.5	3.5	2	1052	82
800	1.3	5.0	2	1200	91

**Table 2.1 :** Textural and morphological characteristics of the ZnO

Figure 2.8 shows the adsorption-desorption isotherms for samples S1 treated at different temperatures. The material has characteristic of non-porous nanoparticulate material only until heating temperatures of 600°C. (type II isotherm, according to BDDT [19] classification). The hysteresis type H3 is associated with a closure of the hysteresis loop due to the so-called tensile strength effect, provoked by particles platelike, according to the SEM images. This characteristic disappears with the increase in the heating temperature due to the growth and densification of the material.

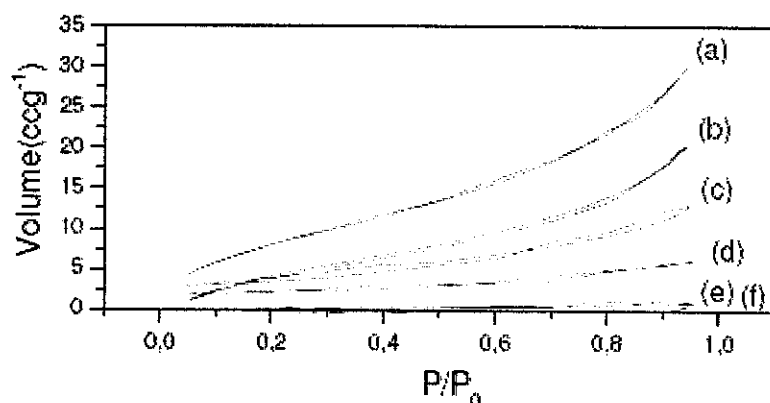


**Fig 2.8:** Adsorption-desorption isotherms of ZnO nanoparticles (S1) treated at different temperatures: (a) 110°C, (b) 200°C, (c) 400°C, (d) 600°C, (e) 800°C and (f) 1000°C

The freeze drying materials showed irregular isotherm curves (not shown), with C constant negative, characteristic of small interaction of the nitrogen with the material. We observed that the nitrogen did not wet the ZnO surface, showing that this kind of drying change significantly the surface sample, confirming the IR results.

#### **2.4 ZnO nanoparticles. ZnO Band Gap and Electrical Resistivity.**

Figure 2.9a shows the room temperature optical absorbance spectrum of the ZnO nanowires recorded by dispersing the ZnO nanoforms in spectroscopic grade ethanol. All the samples showed almost similar nature in the optical absorption spectra.

A sharp transition at 373 nm corresponding to 3.324 eV was observed in the optical absorbance spectrum. This corresponds to the bulk value of the band gap of ZnO. The absorption study revealed that the nanoforms were transparent in the visible region. Figure 2.9b shows the room temperature PL spectra of the ZnO nanonail and nanowire arrays with a 300 nm excitation wavelength. The PL spectrum shows a very weak UV and a strong, broad green emission peak at 3.25 and 2.49 eV, respectively. The zoomed view of the UV emission is shown in the inset of Figure 2.9b. The UV emission originated from the excitonic recombination corresponding to the band edge emission of ZnO. The origin of green luminescence from the undoped ZnO is associated with the intrinsic defect centers such as oxygen vacancy (VO), zinc vacancy (VZn), zinc interstitial (Zni), oxygen interstitial (Oi), or antisite oxygen (OZn). Though the origin of the green emission is generally referred to the deep level or trapped state emission, there is no universally accepted mechanism. There are few hypotheses to explain the origin of the green emission. The commonly cited reason is that the green emission originates due to the radiative recombination of a photogenerated hole with an electron occupying the oxygen vacancy. The green luminescence might be due to the transition from the conduction band to the deeply trapped hole. The donor-acceptor transitions are also reported [30][31] to be the origin of green emission. Complex defects involving transition from the zinc interstitial to the deep acceptor level like oxygen vacancy is another reason reported behind the green emission [32][33]. It is reported that oxygen antisite (OZn) could also induce green emission from ZnO [46].



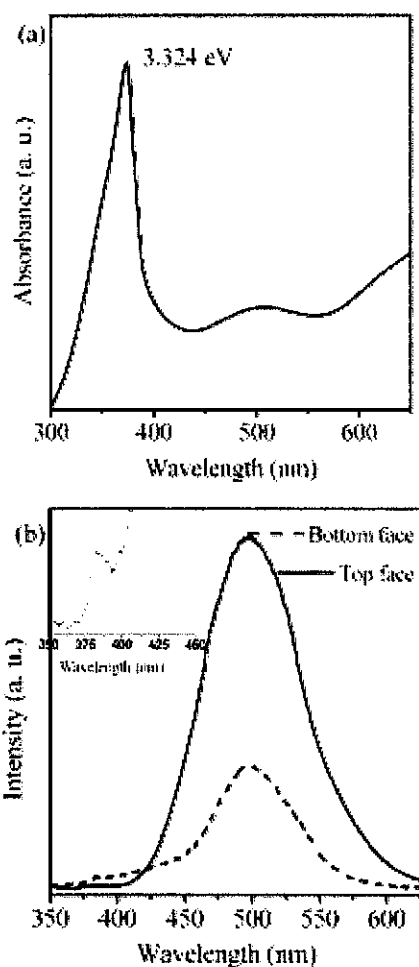


**Figure 2.9.** (a) Room temperature optical absorption spectrum of the ZnO nanowires. (b) Room temperature PL spectra of the ZnO nanonails and nanowire arrays.

It was observed that the emission from the top surface was much stronger than that of the bottom surface. Despite the fact that our sample has been prepared in an oxygen rich atmosphere, EDAX revealed oxygen deficiency in the samples. So, we believe that the transition from the conduction to the deep-level acceptor state is the reason behind the green emission from our samples. These PL spectra and the EDAX results also support our view about the self-catalyzed action of the Zn to form ZnO nanowire/nanonail arrays. When the synthesis was stopped suddenly the top portion of the 1-D ZnO nanoforms remained Zn rich and as a result the possibility of the

generation of deep level defect centers such as oxygen vacancy and Zn interstitials increased.

In Figure 2.10 is shown the variation of log resistance as a function of inverse temperature for the sample characterized by the microstructure of Figure 2.11b. This is typical of all the samples studied. It is evident that the resistance variation reflects an activated process with the activation energy showing a variation with temperature. There are insufficient data, however, to be able to extract reliable terminal values of the activation energy. Figure 2.11a shows the typical resistance change of a sample as a function of time when it was subjected to a gas mixture with N<sub>2</sub> of 200 ppm of CO at a temperature of 225 °C. It can be seen that the resistance decreases by a factor of ~1.7. This arises because of the following reaction



which injects electrons into the conduction band. As a result the electron conductivity increases. Figure 2.11b gives the resistance change with respect to time when sample was kept in an stream of 200 ppm of NO<sub>2</sub> in N<sub>2</sub> at a temperature of 225 °C. It is evident that there is an increase of resistance by a factor of 2. This can be explained on the

basis of the following reaction



The interstitial Zn atoms are oxidized to ZnO. This reduces the donor atoms, which in turn decreases the number of conduction electrons. Thus the electrical resistivity increases drastically. In Figure 2.11c is shown the resistance change of the sample exposed to a gas stream containing 100 ppm of H<sub>2</sub>S in N<sub>2</sub> at a emperature of 100 °C. It is seen that there is a decrease of sample resistance by a factor of 1.4. This happens because of the reducing action of the H<sub>2</sub>S, which injects electrons in the conduction band. The reaction concerned can be visualized as follows,



It should be noted, however, that the sensing response is non-specific. More data have to be collected as a function of the concentration of the different gaseous species before a firm conclusion regarding the gas sensing applications of these materials can be drawn.

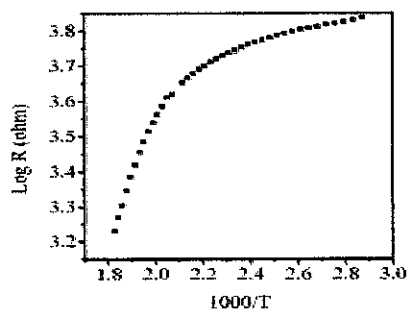


**Figure 2.10.** Log resistance versus inverse temperature plot for the ZnO nanonail array.

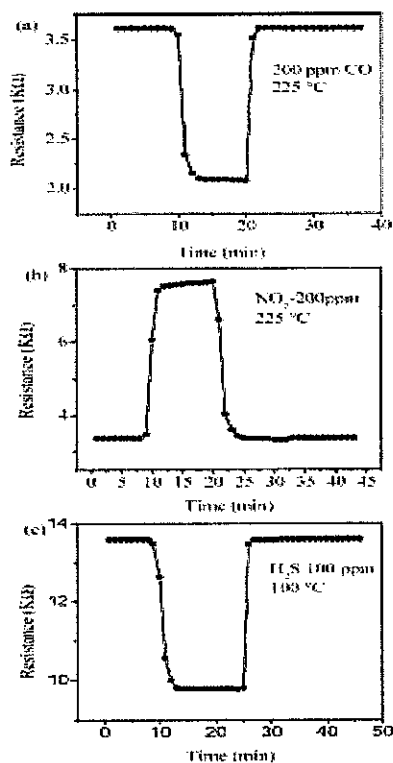


**Figure 2.11.** Change of dc resistance of the ZnO nanonail array as a function of time in different gases at different concentrations and temperatures: (a) 200 ppm of CO at 225 °C, (b) 200 ppm of NO<sub>2</sub> at 225 °C, and (c) 100 ppm of H<sub>2</sub>S at 100 °C.

By referring to an experiment done by mixing TiO and ZnO, such as combination is entirely sensible as zinc oxide absorbs more strongly in the UVA range and titanium dioxide more strongly in the UVB range, which would mean that broadband absorption could be achieved over the entire UV range. However these two substances have different isoelectric points: TiO<sub>2</sub> approximately 5 to 6 and ZnO approximately 9.5. At a pH value of between 5 and 7, which is typical for cosmetic products, oppositely charged particles may be present, which attract each other and may result in agglomeration or flocculation. This risk primarily occurs when both metal oxides are present in the aqueous phase. Combining zinc oxide and titanium dioxide is to provide a powder which combines the advantages of zinc oxide and titanium dioxide. The combination provides a powder mixture consisting of zinc/titanium mixed oxide particles, titanium dioxide particles and zinc oxide particles are obtained from a thermal process and wherein the powder mixture exhibits remission which, in the UV range from 320 to 400nm is lower than that of titanium dioxide and in the UV range below 320 nm, is lower than that of zinc oxide. It may furthermore be advantageous if the isoelectric point of the powder mixture according to the invention is between that of zinc oxide and titanium oxide. The isoelectric point of zinc oxide is at approx. 9.2 that of titanium dioxide at approx. 5-6. the titanium dioxide particles of the powder mixture according to the invention may have rutile, anstase and brokrite modifications, the ratio of which to one another is not limited. Preferably, however, the proportion of the rutile modification of the titanium dioxide materials of the powder mixture according to the invention may amount to at least 1% relative to the sum of rutile and anatase modification [5].

### **2.5 Effect of Different Ratios of Mixture Used**

Figure 2.12 shows the XRD patterns of the ZnO films with 300 nm in thickness. It is revealed that the films consist of polycrystalline materials in the Zn-rich region where Zn/(Zn + In) ratio is above 67 at%, while the films are amorphous at lower Zn contents. For crystal structures of the ZnO–In<sub>2</sub>O<sub>3</sub> system, we assign these peaks observed at higher Zn contents to c-axis oriented homologous phases Zn<sub>k</sub>In<sub>2</sub>O<sub>3(k+3)</sub>.

Specifically, the diffraction peaks observed at the Zn/(Zn + In) ratios of 67 at% and 69 at% correspond to  $k = 5$ , while the peaks observed at Zn/(Zn + In) ratios of 83 at% and 87 at% correspond to  $k = 11$ . It should be noticed that the best compositional ratio mentioned above is located near the boundary between the crystalline and amorphous phases. Hence, we took transmission electron microscopy (TEM) images of the TFTs to confirm the structures of the ZiO films used for the channel layers.

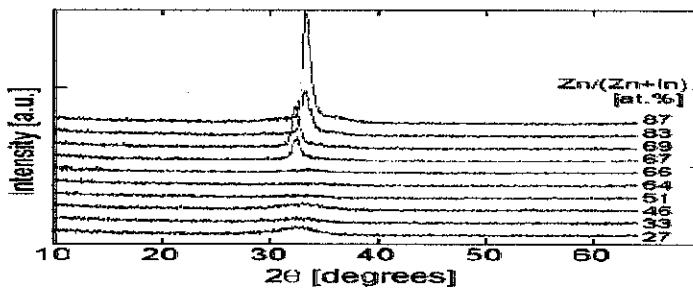


**Figure 2.12** : XRD patterns of ZiO films for different In:Zn ratios.

Figure 2.13 shows the cross sectional TEM images on the specimens with Zn: In ratios of 70:30 and 60:40. It is seen clearly that the film with the Zn: In of 60:40, which exhibited the best TFT performance, has a homogeneous amorphous structure. On the other hand, the film with the Zn: In of 70: 30, has a polycrystalline structure. Therefore, the degradation of the TFT characteristics with increasing the Zn ratio is considered to be partly due to the polycrystalline structure, i.e., the grain boundaries, which may form the gap states and interface states, deteriorate the TFT performances, especially  $\mu_{\text{sat}}$  and S.S. Furthermore, the large negative  $V^{\text{th}}$  observed at the Zn: In ratio of 70:30 can be attributed also to the polycrystalline structure. One possible reason is that the In substitution of the Zn sites in the crystallized ZiO films provides excess electron carriers in addition to those generated by oxygen vacancies as observed in related crystalline films which makes  $V^{\text{th}}$  largely negative. Another possible reason is as follows. It is known that the n-type transparent conductive oxides such as polycrystalline ZnO and  $\text{In}_2\text{O}_3$  have high residual carrier concentration that is difficult to be reduced. It is reported that ZnO films with a low residual carrier concentration ( $\sim 10^{15} \text{ cm}^{-3}$ ) can be realized by decreasing the grain boundary density,

which suggests that many of the carriers in n-type oxide films come from the defects at the grain boundaries. Therefore, the polycrystalline ZIO films can have high carrier density, which results in the large negative  $V_{th}$  of the ZIO-TFTs. In fact, we have observed in Hall measurements that the carrier concentration of the ZIO films with the Zn: In ratio of 70:30 is higher than that with the Zn: In ratio of 60:40. The electrical resistivity of the ZIO films was also measured using a four-point probe method.

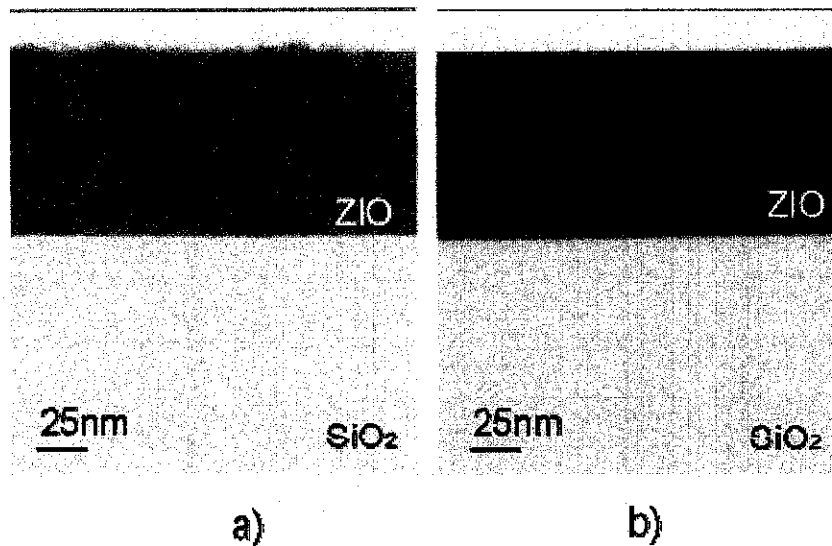


**Figure 2.13** Cross sectional TEM images of ZIO channel layers with Zn/(In + Zn) of a) 70 at% and b) 60 at%.

Figure 2.14 shows the compositional dependence of the ZIO film resistivity and their time variation. Here, the relative humidity was kept at 45% and the temperature was room temperature in the storage atmosphere. The  $O_2$  partial pressure in the deposition atmosphere was 5.7 mPa. It is seen that shortly after the film preparation, the resistivities drastically decrease with time and the decreases become smaller with time. Ultimately, the resistivities hardly change with time. The reason of this instability is still under study. However, it was observed that for the films with the same Zn: In ratio, even if the initial resistivities are different, the final resistivities tend to be the same, where the resistivities hardly change. These results suggest that

the resistivities of ZnO films have the specific values determined by the Zn: In ratio and do not go below these values. Hereafter, we discuss the compositional dependence of the resistivity measured 3 months after preparation. It is found that the semi-conductive ZnO films whose resistivities are in the range of 10–10<sup>3</sup> Ω cm (note that it is reported that In–Ga–Zn–O TFTs show switching behaviours at least in this resistivity range) are obtained only at low In ratios. While, the resistivity decreases with increasing the In ratio and becomes lower than 1 Ω cm when the In ratio exceeds 50 at%. Hall measurements revealed that this low resistivity is mainly due to the increase in the electron carrier density with time. Hence, the poor TFT characteristics, such as low I<sub>on</sub>/I<sub>off</sub> and large negative V<sub>th</sub>, observed at the high In ratios, are attributed to too high carrier density, which may come from the formation of oxygen vacancy, and so on. It should also be noted that despite the increase in the carrier density with the Zn ratio from 60 at% to 70 at%, the resistivity changes little, which is due to the decrease in the Hall mobility with the Zn ratio. The stability of the ZnO-TFTs in an ambient atmosphere was also examined for different Zn: In ratios at room temperature in a 45% humidity air.

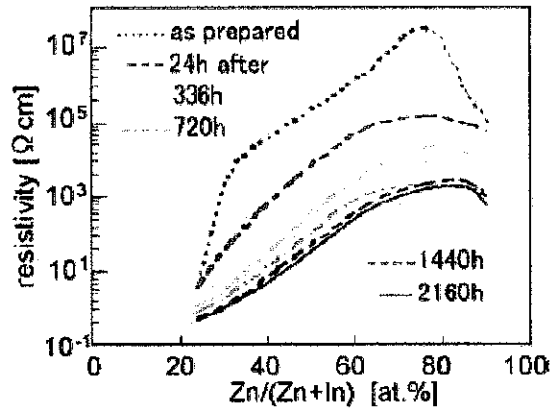


**Figure 2.14** Compositional dependence of film resistivity. The numbers indicated in the legend denote the passing time in hours after the deposition of the film.

Figure 2.15a shows the changes in the threshold voltage V<sub>th</sub> during 3 months after the TFT fabrication. The air stability also depends on the Zn: In ratio. Not large, but

finite  $V^{\text{th}}$  shifts were observed for most of the TFTs fabricated here, which is consistent with the results of time variation measurement of the ZIO film resistivity mentioned above. However, the TFT having the Zn: In ratio of around 60:40 shows very small  $V^{\text{th}}$  shift. It should be noted that the best TFT performances were obtained at the same composition ratio. Figure 2.15b shows the transfer characteristics of the ZIO-TFTs with the Zn: In ratio of 60:40. The dashed and solid lines represent the initial transfer characteristic and that measured after the 3 months stability test, respectively. It shows that the TFT characteristics exhibit little changes. Recently, it has been reported that the air stability of ZIO films is not good, which makes ZIO-TFTs less attractive compared with IGZO-TFTs. In fact, we observed that the resistivity of the ZIO films changes with time. However, our results indicate that high air stability is obtained even for ZIO-TFTs if we carefully choose the appropriate composition ratio, at which the high-performance TFTs can also be obtained.

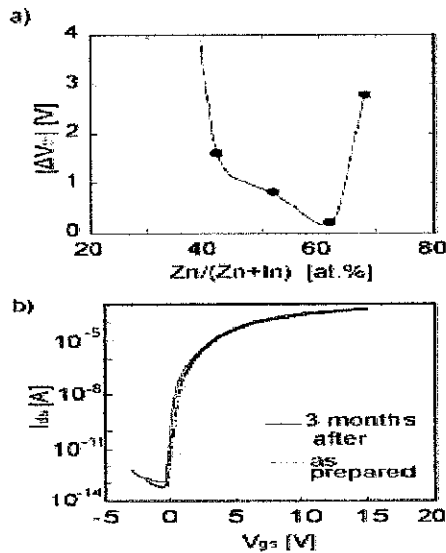


**Figure 2.15** Effect of duration on ZIO-TFTs performances. a) Compositional dependence of  $V^{\text{th}}$  shift. Here,  $|\Delta V^{\text{th}}|$  denotes the absolute differences between the initial  $V^{\text{th}}$  and  $V^{\text{th}}$  measured after the 3 months stability test. b) Transfer characteristics of ZIO-TFT with the Zn: In ratio of 60: 40. The dashed and solid lines



represent the initial transfer characteristic and that measured after the 3 months stability test, respectively.

## 2.6 About of NiO

Nickel(II) oxide is the chemical compound with the formula NiO. It is notable as being the only well characterized oxide of nickel although (nickel(III) oxide,  $\text{Ni}_2\text{O}_3$  and  $\text{NiO}_2$  have been claimed.[38] The mineralogical form of NiO, bunsenite, is very rare. It is classified as a basic metal oxide. Several million kilograms are produced in varying quality annually, mainly as an intermediate in the production of nickel alloys.[39]. NiO can be prepared by multiple methods. Upon heating above 400 °C, nickel powder reacts with oxygen to give NiO. In some commercial processes, green nickel oxide is made by heating a mixture of nickel powder and water at 1000 °C, the rate for this reaction can be increased by the addition of NiO.[40] The simplest and most successful method of preparation is through pyrolysis of a nickel(II) compounds such as the hydroxide, nitrate, and carbonate, which yield a light green powder.[38] Synthesis from the elements by heating the metal in oxygen can yield grey to black powders which indicates nonstoichiometry.[38]. NiO adopts the NaCl structure, with octahedral Ni(II) and  $\text{O}_2^-$  sites. The conceptually simple structure is commonly known as the rock salt structure. Like many other binary metal oxides, NiO is often non-stoichiometric, meaning that the Ni:O ratio deviates from 1:1. In nickel oxide this non-stoichiometry is accompanied by a color change, with the stoichiometrically correct NiO being green and the non-stoichiometric NiO being black. NiO has a variety of specialized applications and generally applications distinguish between "chemical", which is relatively pure material for specialty applications, and "metallurgical grade", which is mainly used for the production of alloys. It is used in the ceramic industry to make frits, ferrites, and porcelain glazes. The sintered oxide is used to produce nickel steel alloys. Charles Édouard Guillaume won the 1920 Nobel Prize in Physics for his work on nickel steel alloys which he called invar and elinvar. NiO was also a component in the Nickel-iron battery, also known as the Edison Battery, and is a component in fuel cells. It is the precursor to

many nickel salts, for use as specialty chemicals and catalysts. More recently, NiO was used to make the NiCd rechargeable batteries found in many electronic devices until the development of the environmentally superior Lithium Ion battery.[40]. About 4000 tons of chemical grade NiO are produced annually.[39] Black NiO is the precursor to nickel salts, which arise by treatment with mineral acids. NiO is a versatile hydrogenation catalyst. Heating nickel oxide with either hydrogen, carbon, or carbon monoxide reduces it to metallic nickel. It combines with the oxides of sodium and potassium at high temperatures ( $>700^{\circ}\text{C}$ ) to form the corresponding nickelate.[40]

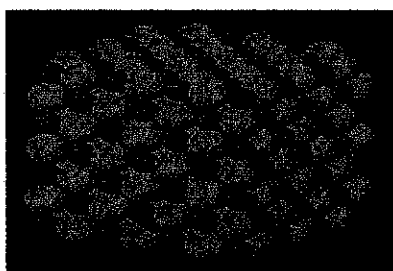


**Figure 2.16 :** Nickel Oxide Structure.

## **2.7 Properties of Nickel Oxide**

Surface morphology was studied by JEOL GSM-5900 scanning electron microscope [41]. The transmission electron micrographs were taken with a JEOL JEM-2010 electron microscope. The phase and crystallinity were characterized by using a Rigaku X-ray diffractometer with Cu K radiation over a range of  $2\theta$  angles from  $30$  to  $70^{\circ}$ . Raman scattering was measured at room temperature using Renishaw Raman microscope with Ar<sup>+</sup> laser operating at 514.5 nm. UV-visible absorption spectrum was obtained from Varian Cary 3E spectrophotometer in the range 200–600 nm. FT-IR spectra of the nanoparticles (as pellets in KBr) have been recorded in BIO-Rad Win instrument.

### Scanning electron microscopic images

Fig. 2.17 shows the SEM image of NiO nanoparticles synthesized by using nickel acetate/PVAc precursor heat treated at 723 K. From this image it is clearly seen that the NiO particles have nearly uniform size and well dispersion in the bulk state with diameter around 40–50 nm. This indicates that PVAc played a key role in the formation of well-dispersed nanoparticles by avoiding their aggregation due to coordination with nickel ion in the composite mixture that leads to the formation of uniform sized NiO during heat treatment in air.

### Transmission electron microscopy

Transmission electron micrographs have been recorded using a copper grid dipped in a solution containing NiO nanoparticles dispersed in ethanol by ultrasonication and presented in Fig. 2.18. TEM photos revealed the presence of a large number of NiO particles with hexagonal shape and uniform size around 40–50 nm and well dispersed in the bulk material. Inset in this figure shows the electron diffraction pattern of the selected area of nanoparticles. The appearance of strong diffraction spots rather than diffraction rings confirmed the formation of single crystalline cubic nickel oxide.

### X-ray diffraction studies

The typical XRD pattern of NiO nanoparticles obtained after heat treatment at 723K is presented in Fig. 2.19. The existence of strong and sharp diffraction peaks at  $2\theta$  values 37.25, 43.30 and 62.90° corresponding to (1 1 1) (2 0 0) and (2 2 0) crystal planes indicated the formation of phase pure, cubic nickel oxide (bunsenite, NaCl type structure) at this temperature. The particle size of the prepared nickel oxide calculated from XRD using the Debye–Sherrer equation is about 43.92 nm, in good agreement with that observed from TEM images. The nature and positions of the above diffraction peaks are characteristic of cubic nickel.

### Raman spectrum

Fig. 2.20 shows the Raman spectrum of NiO nanoparticles synthesized in this study. The Raman spectrum exhibited a strong, broad peak at  $518\text{ cm}^{-1}$  due to the NiO stretching mode

### UV-visible spectrum

Fig. 2.21 shows the UV-visible absorption spectrum of NiO nanoparticles obtained after heat treatment at 723 K. It can be seen that the absorption edge corresponding to NiO appeared at 320 nm.

### FT-IR spectra

The formation of pure nickel oxide nanoparticles after heat treatment at 723K was also identified by FT-IR spectral studies (Fig. 2.22). The spectrum of nickel acetate/PVAc precursor showed some strong absorption in the region  $1200\text{--}1800\text{ cm}^{-1}$  that can be assigned to PVAc molecule (curve a). The samples obtained after heating at 723K did not exhibit any such bands thereby confirming the complete removal of PVAc at this temperature, but new peaks were found at  $445$  and  $490\text{ cm}^{-1}$  (curve b). These peaks were undoubtedly assigned to NiO stretching as was reported earlier by other researchers.

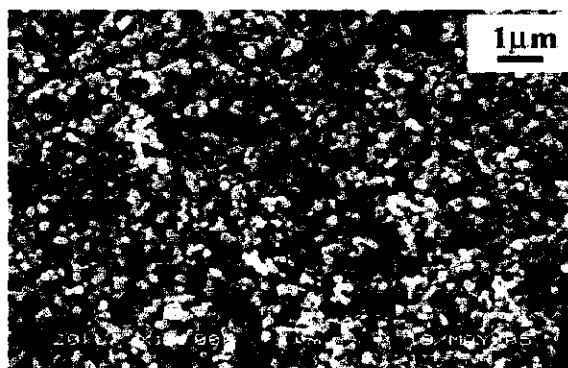
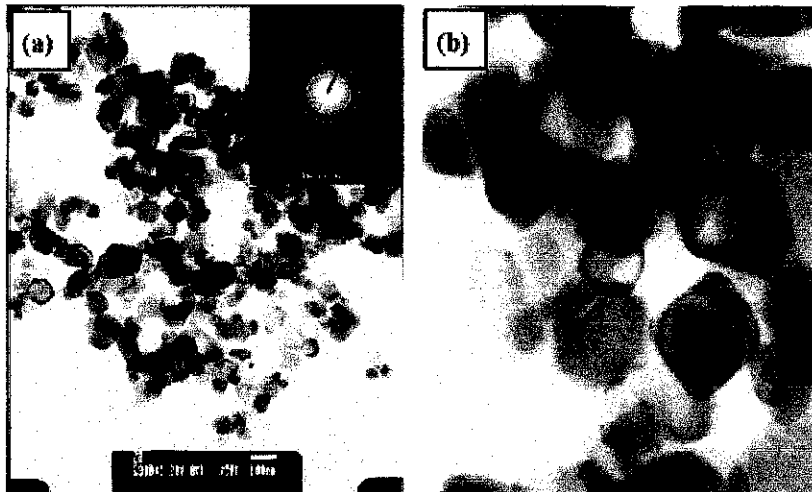
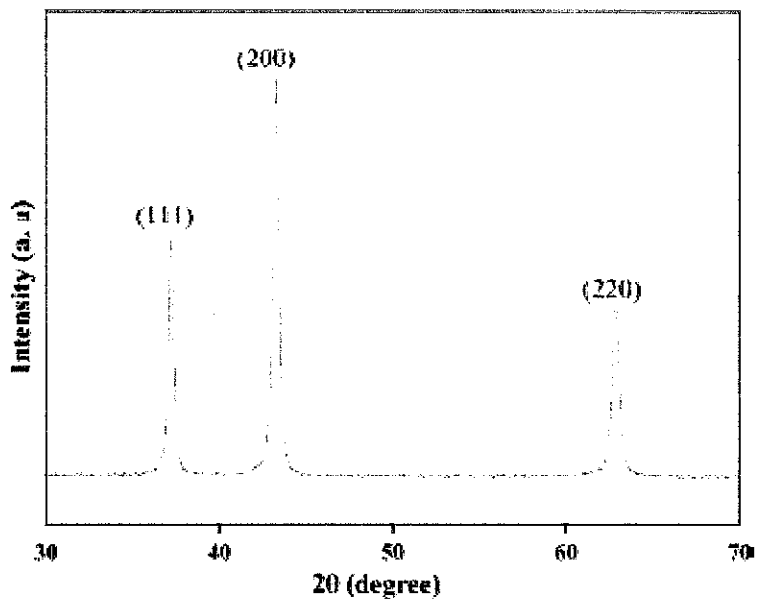


Fig. 2.17. Scanning electron microscopic (SEM) image of NiO nanoparticles.



**Fig. 2.18.** Transmission electron microscopic (TEM) images of NiO nanoparticles; (a) lower magnification and (b) higher magnification (inset in (a) showed the selected area electron diffraction pattern).



**Fig. 2.19.** XRD pattern of NiO nanoparticles.

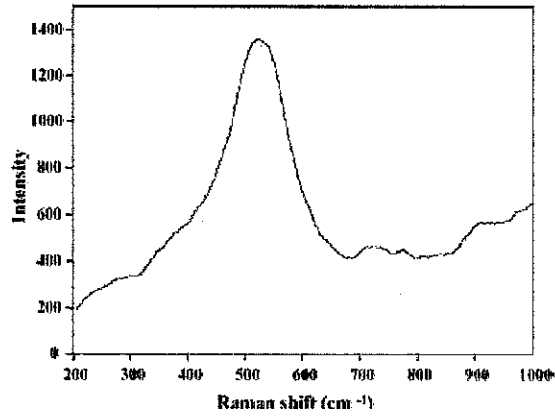


Fig. 2.20. Raman spectrum of NiO nanoparticles.

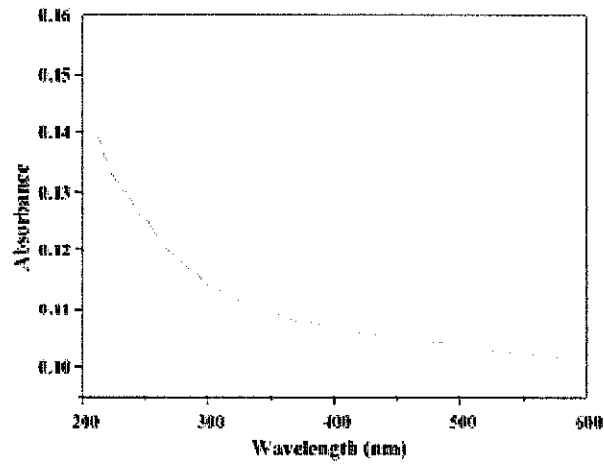


Fig. 2.21 UV-visible absorption spectrum of NiO nanoparticles.

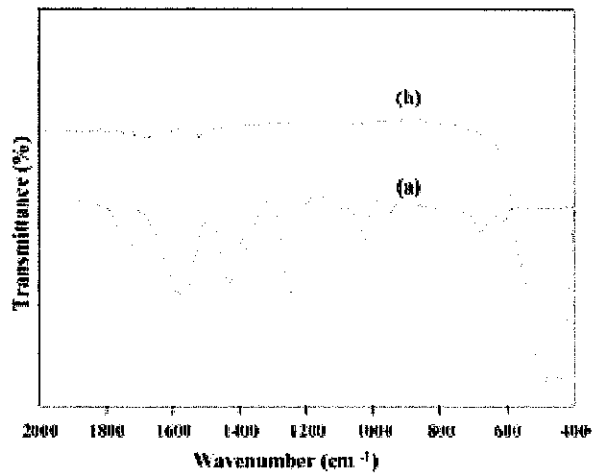


Fig. 2.22. FT-IR spectra: (a) nickel acetate/PVAc precursor and (b) NiO nanoparticles.

Cubic nickel oxide nanoparticles with diameter around 40–50 nm were synthesized from nickel acetate/PVAc precursor by heat treatment at 723 K. The particles were found to have size-homogeneity and well dispersed in the bulk, which was attributed to the presence of coordinated PVAc with nickel ion in the precursor and prevents the aggregation of nickel oxide into bulk mass during heat treatment. Though the particle size of NiO seems to be little large, the size uniformity and fine dispersion of the particles were significant aspects of this project.

## 2.8 Reflux

Reflux is a technique involving the condensation of vapors and the return of this condensate to the system from which it originated. It is used in industrial and laboratory distillations. It is also used in chemistry to supply energy to reactions over a long period of time. The term reflux [42][43] is very widely used in industries that utilize large-scale distillation columns and fractionators such as petroleum refineries, petrochemical and chemical plants, and natural gas processing plants. In that context, reflux refers to the portion of the overhead liquid product from a distillation column or fractionator that is returned to the upper part of the column. The more reflux provided for a given number of theoretical plates, the better is the column's separation of lower boiling materials from higher boiling materials. Conversely, for a given desired separation, the more reflux is provided, the fewer theoretical plates are required.

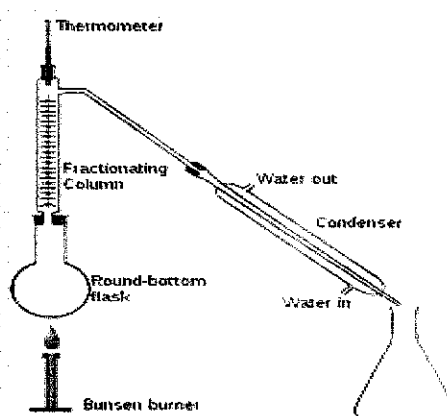
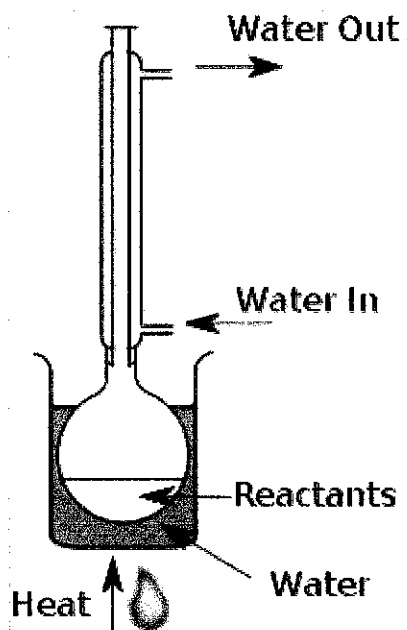


Fig. 2.23 Reflux Set

The apparatus shown in the diagram represents a batch distillation as opposed to a continuous distillation. The liquid feed mixture to be distilled is placed into the round-bottomed flask along with a few anti-bumping granules, and the fractionating column is fitted into the top. As the mixture is heated and boils, vapor rises up the column. The vapor condenses on the glass platforms (known as plates or trays) inside the column and runs back down into the liquid below, thereby refluxing the upflowing distillate vapor. The hottest tray is at the bottom of the column and the coolest tray is at the top. At steady state conditions, the vapor and liquid on each tray is at equilibrium. Only the most volatile of the vapors stays in gaseous form all the way to the top. The vapor at the top of the column then passes into the condenser, where it cools until it condenses into a liquid. The separation can be enhanced with the addition of more trays (to a practical limitation of heat, flow, etc.). The process continues until all the most volatile components in the liquid feed boil out of the mixture. This point can be recognized by the rise in temperature shown on the thermometer. For continuous distillation, the feed mixture enters in the middle of the column.



**Figure 2.24 Common Reflux Preparation**



A liquid reaction mixture is placed in a vessel open only at the top. This vessel is connected to a Liebig condenser, such that any vapours given off are cooled back to liquid, and fall back into the reaction vessel. The vessel is then heated vigorously for the course of the reaction. The purpose is to thermally accelerate the reaction by conducting it at an elevated temperature (i.e. the solvent's boiling point). The advantage of this technique is that it can be left for a long period of time without the need to add more solvent or fear of the reaction vessel boiling dry as any vapour is immediately condensed in the condenser. In addition, as a given solvent will always boil at a certain temperature, one can be sure that the reaction will proceed at a constant temperature. By careful choice of solvent, one can control the temperature within a very narrow range. The constant boiling action also serves to continuously mix the solution, although a magnetic stirring rod mechanism is often used to achieve a uniform solution. This technique is useful for performing chemical reactions under controlled conditions that require substantial time for completion. By controlling the temperature of the condenser, a reflux still may be used to ensure that higher boiling point components (which are also of higher molecular weight) are returned to the flask while lighter elements are passed out to a secondary condenser. This is useful in producing high quality alcoholic beverages, while ensuring that less desirable components (such as fusel alcohols) are returned to the primary flask. This is particularly effective in the production of alcoholic beverages in which it is appropriate to retain the flavors and aromas of the source fruit - such as applejack. For high quality neutral spirits (such as vodka), or post distillation flavored spirits, a process of multiple distillations or charcoal filtering may be applied to obtain a product lacking in any suggestion of its original source material for fermentation.

## **CHAPTER 3**

### **METHODOLOGY**

#### **3.1 Research Methodology**

First, the problem is defined to determine the main objective of the project. Next, literatures are reviewed in order to get the ideas or theory related to the project. Then, possible hypothesis are formulated to initiate the project and based on the hypothesis, experimental processes are design. After that, data is started to be collected and results are analyzed. Finally, the conclusion of the project is determined based on the laboratory analyzed results.

#### **3.2 Project Activities**

There are two experiments involved in order to complete the project purpose:

- 1) The effect of Zinc Oxide to Nickel Oxide ratio
- 2) The effect of different calcinations temperature

##### **3.2.1 The Effect of Zinc Oxide to Nickel Oxide ratio**

The ratio will be varied as:

1. 0.2 mol Zinc Chloride and 0.2 mol Nickel(ii)Nitrate
2. 0.5 mol Zinc Chloride and 0.2 mol Nickel(ii)Nitrate
3. 0.2 mol Zinc Chloride and 0.5 mol Nickel(ii)Nitrate
4. 0.2 mol Zinc Chloride and 0.7 mol Nickel(ii)Nitrate

##### **3.2.2 The Effect different calcination temperatures**

The calcination temperatures will be varied for 400°C, 500°C and 600°C

### **3.3 Chemicals List**

#### **3.3.1 Zinc Chloride**

The chemical will be weighted according to ratio used and then will be mixed with portion of Nickel(ii) Nitrate.

#### **3.3.2 Nickel(ii)Nitrate**

The chemicals will be weighted according to ratio used and then will be mixed with portion of Zinc Chloride.

### **3.4 Equipment List**

#### **3.4.1 Hot Plate**

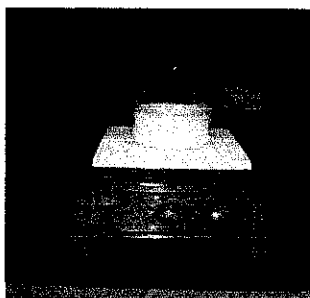


**Figure 3.25 : Hot plate**

This equipment is used to heat the mixture of Zinc Chloride and Nickel(ii) Nitrate with the additional chemical. The heating purpose is to favor reactions between two chemicals inside the solution, before reflux process.

#### **3.4.2 Reflux set-up**

Reflux set-up is shown from the figure below:

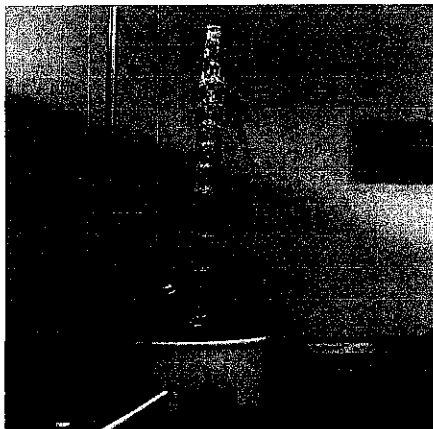


**Figure 3.26: Reflux Set-up**

The experiments exploit the benefit of reflux process, whereby it can apply high energy to favor the chemical reaction, without having the fear of the solution might get dried after long hour of heating process.

### **3.4.3 Vacuum Filter**



**Figure 3.27 : Vacuum Filter**

This equipment is used to filter the refluxed mixture.

### **3.4.3 Scanning Electron Microscope (SEM)**

This equipment is used to take images of the surface of the final products. It can produce very high-resolution images of a sample surface, revealing details about less than 1 to 5 nm in size. SEM images are used to examine the effect of variables selected towards crystal morphology.

#### **3.4.4 X-Ray Diffractometer**

X-ray diffraction (XRD) method is used to examine the crystal structure and orientation of the final product.

#### **3.4.5 Ultraviolet-visible Spectroscope (UV-VIS)**

UV-VIS is used to examine the band gap, wavelength and optical transmittance measurement of the final product. The final product is obtained and compared.

### **3.5 Experiment Procedures**

#### **3.5.1 Effect of different ratio of Zinc Oxide to Nickel (ii) Nitrate**

1. 0.2 mol zinc chloride, 0.2 mol nickel(ii) nitrate, and 100 ml of distilled is mixed in a beaker
2. The mixture will be heated up on a hot plate while covered by a layer of aluminum foil for 3 hours and without the cover of aluminum foil for another 3 hours. The temperature is maintained at 800°C
3. The heated mixture will be transferred to reflux set apparatus
4. Boiling chips is added together with the heated mixture.
5. The solution will be heated for 4 hours at 110°C
6. The solution then will be filtered until desired product is achieved.
7. The product then will be dried in the oven until we get dry solution.
8. The dried solution will be treated in a furnace at 400°C for 16 hours.
9. Samples will be tested at SEM,XRD and also UV-VIS
10. Step 1 until 9 is repeated using different portion of zinc chloride and nickel nitrate

### **3.5.2 Effect of different calcination temperatures**

Steps 1 to 9 as Experiment 3.5.1 are repeated using 2 more different calcinations temperatures which are 500°C and 600°C at step 8.

### **3.5.3 Experiment Variables**

Ratios of Zinc Chloride to Nickel (ii) Nitrate

5. 0.2 mol Zinc Chloride and 0.2 mol Nickel(ii)Nitrate
6. 0.5 mol Zinc Chloride and 0.2 mol Nickel(ii)Nitrate
7. 0.2 mol Zinc Chloride and 0.5 mol Nickel(ii)Nitrate
8. 0.2 mol Zinc Chloride and 0.7 mol Nickel(ii)Nitrate


Calcination temperatures

1. 400°C
2. 500°C
3. 600°C

3.6 Project Process Flow (Gantt Chart)

Table 3.2: Gantt Chart for FYP II

No.	Detail/Week	1	2	3	4	5	6	7	8	9	10	11	12	13	14
1	Project Work Continue														
2	Submission of Progress Report 1			☆											
3	Project Work Continue														
4	Submission of Progress Report 2								☆						
5	Seminar (compulsory)														
5	Project work continue														
6	Poster Exhibition											☆			
7	Submission of Dissertation (soft bound)												☆		
8	Oral Presentation													☆	
9	Submission of Project Dissertation (Hard)														☆

☆ Suggested milestone  
 Process

## CHAPTER 4

### RESULT AND DISCUSSION

#### 4.1 Result

##### 4.1.1 Experiment 1

Chemical used : 0.2 mol zinc chloride  
0.2 mol nickel(ii)nitrate

A solution of 0.2 mol zinc chloride, 0.2 mol nickel (ii) nitrate, and 100ml of distilled water is prepared, and the is being heated at 80°C and refluxed at 145°C. The solution is then filtered and placed in a furnace for about 14 hours at 450°C, 500°C, and 600°C but there is still no exact result for XRD and SEM since it is still in waiting process for the queue to test all the samples.

From the observation, of solution mixed of zinc chloride, nickel (ii)nitrate and distilled water ,the volume decreases little by little along the heating session. After the reflux process has been conducted, the solution is more concentrated than before. After the sample has been treated in the furnace, the sample changed colour from green to black.

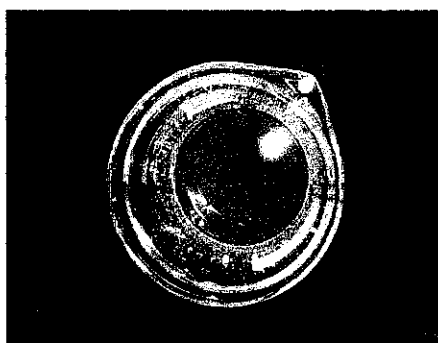
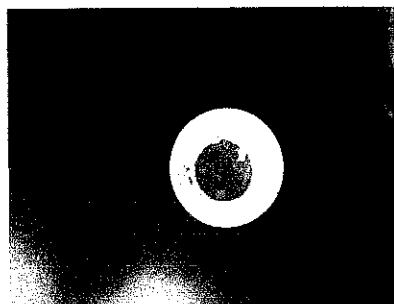
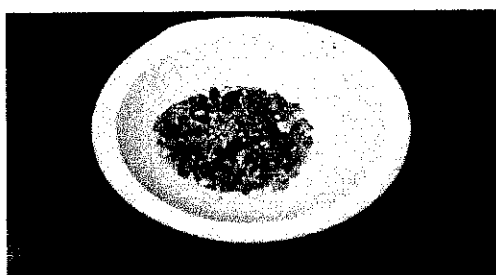


Fig 4.28:Sample after reflux process ( more concentrated than before)





**Fig 4.29** : Sample after filtration



**Fig 4.30** :Sample after being treated in different the furnace

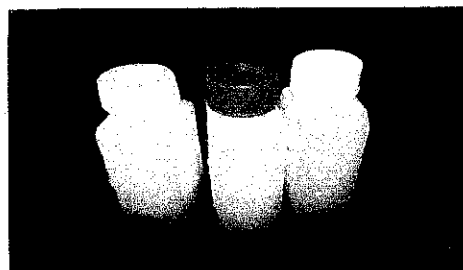


**Fig 4.31**: Samples in three calcinations temperatures

#### **4.1.2 Experiment 2**

Chemical used : 0.5 mol zinc chloride  
0.2 mol nickel(ii)nitrate

A solution of 0.5 mol zinc chloride, 0.2 mol nickel (ii) nitrate, and 100ml of distilled water is prepared, and the is being heated at 80°C and refluxed at 140°C. The solution is then being filtered and placed in a furnace for about 14 hours at 450°C, 500°C, and 600°C but there is still no exact result for XRD and SEM since it is still in waiting process for the queue to test all the samples.

From the observation, of solution mixed of zinc chloride, nickel (ii) nitrate and distilled water, the volume decreases little by little along the heating session.

After the reflux process has been conducted, the solution is more concentrated than the lower ratio of  $ZrO-NiO$  solution and it tends to crystallize in a particular time of period. After the sample has been treated in the furnace, the sample becomes black and little greenish.

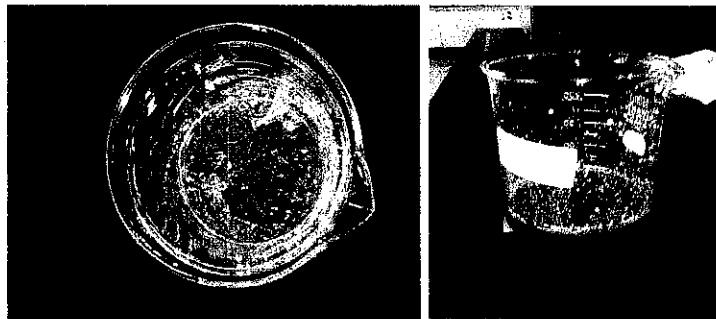


**Fig 4.32** :Sample after reflux process



**Fig 4.33**: Sample after filtration

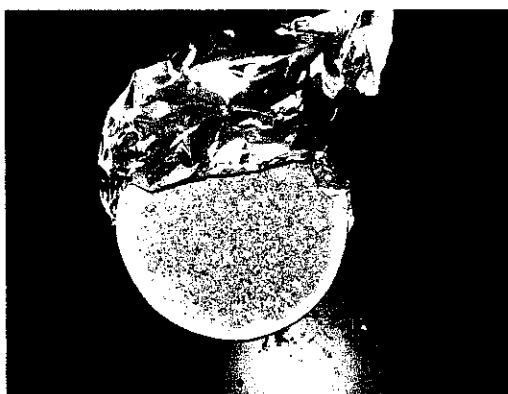


**Fig 4.34** : Sample after being treated in the furnace



**Fig 4.35** : Samples in 3 different calcination temperature

### 4.1.3 Experiment 3

Chemical used : 0.7 mol zinc chloride  
0.2 mol nickel(ii)nitrate

A solution of 0.7 mol zinc chloride, 0.2 mol nickel(ii) nitrate, and 100ml of distilled water is prepared, and the solution is being heated at 80°C and refluxed at 120°C. The solution is then being filtered and placed in a furnace for about 14 hours at 450°C, 500°C, and 600°C but there is still no exact result for XRD and SEM since it is still in waiting process for the queue to test all the samples.

From the observation of solution mixed of zinc chloride, nickel (ii) nitrate and distilled water, the volume decreases little by little along the heating session. After the reflux process has been conducted, the solution is more concentrated than the lower ratio of ZnO-NiO solution and it tends to crystallize and become sticky in a particular time period.



Fig 4.36 : Solution after being refluxed



Fig 4.37: Sample after filtration

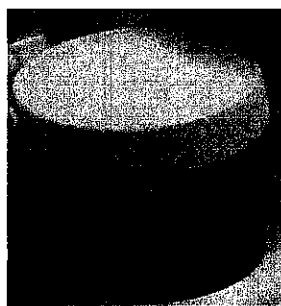


Fig 4.38 Sample after being treated in the furnace

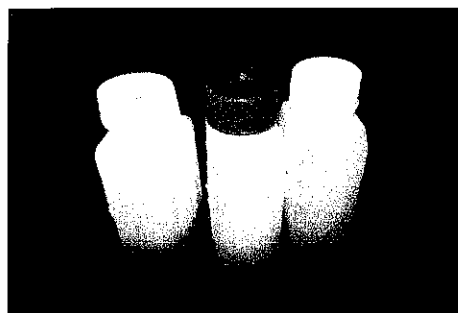
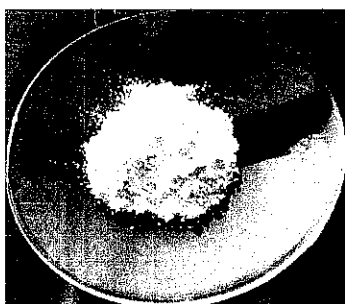


Fig 4.39 Sample in three different calcinations temperatures

#### 4.1.5 Experiment 4

Chemical used : Zinc Chloride



**Figure 4.40:** Zinc Chloride

The experiment was conducted to compare and observe the physico properties of Zinc Oxide itself with other modified nanoparticles. A solution of approximately 0.5 mol Zinc Chloride and 100ml of distilled water is prepared, and the solution is being heated at 80°C and refluxed at 120°C. The solution is then being filtered and placed in a furnace for about 14 hours at 400°C, 500°C, and 600°C but there is still no exact result for XRD and SEM since it is still in waiting process for the queue to test all the samples.

The sample is treated in the furnace at different temperatures and will be tested at UV-Vis, SEM and X-RD.



**Fig 4.41:** Sample at different calcinations temperatures

## 4.2 Uv-Vis result

### Experiment 1

0.2 mol zinc chloride with 0.2 mol nickel(ii)nitrate

at 400°C

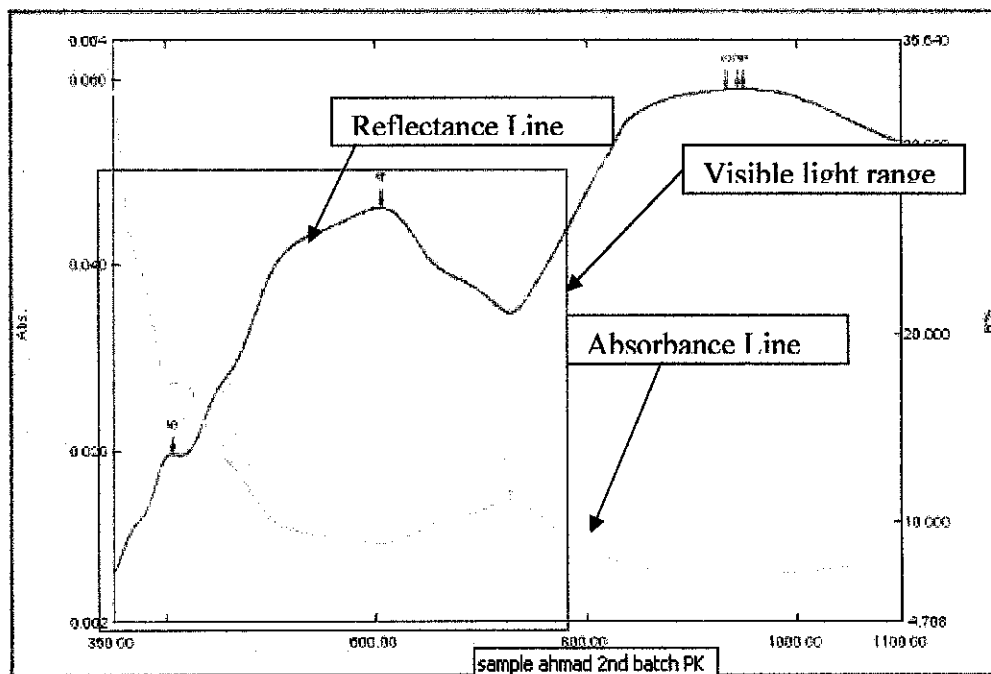


Fig 4.42 0.2 mol zinc chloride with 0.2 mol nickel(ii)nitrate (400 °C)

at 500 °C

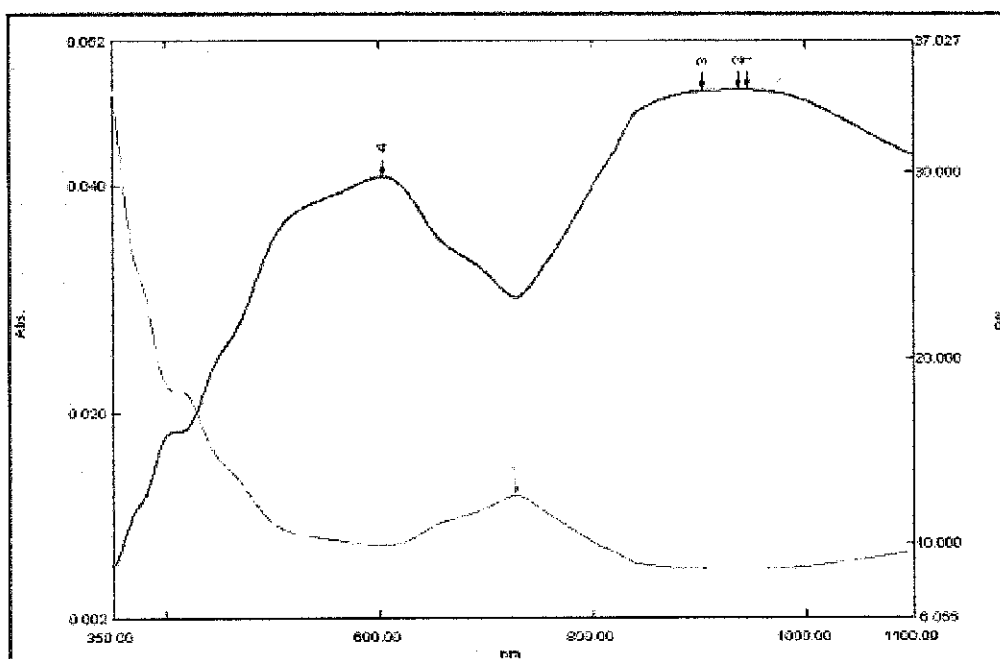


Fig 4.43 0.2 mol zinc chloride with 0.2 mol nickel(ii)nitrate (500°C)

at 600 °C

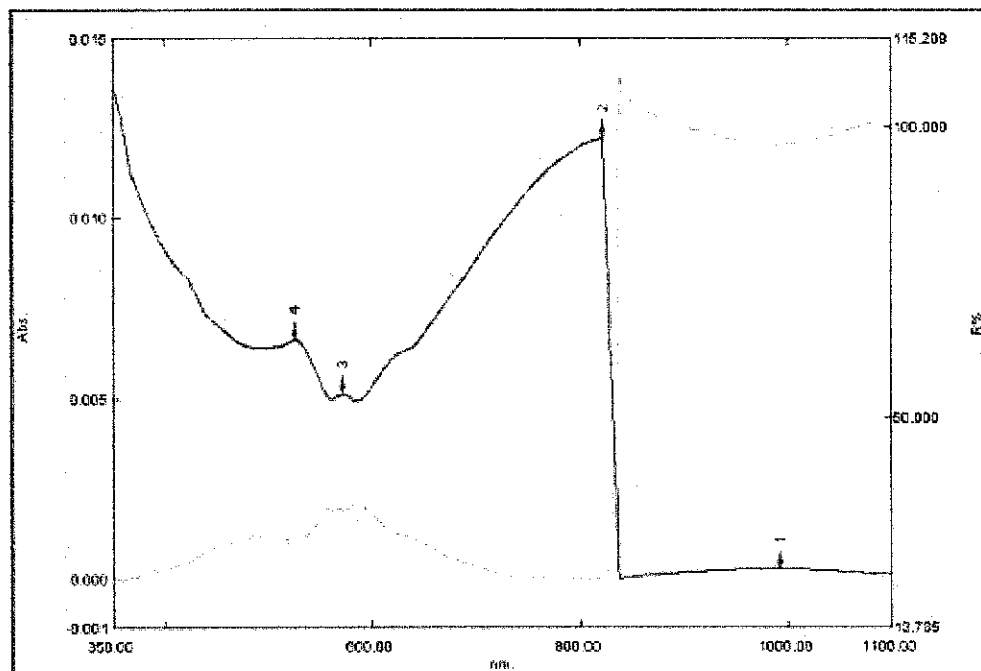


Fig 4.44 0.2 mol zinc chloride with 0.2 mol nickel(ii)nitrate (600 °C)

### Experiment 2

0.5 mol zinc chloride with 0.2 mol nickel(ii)nitrate

at 400 °C

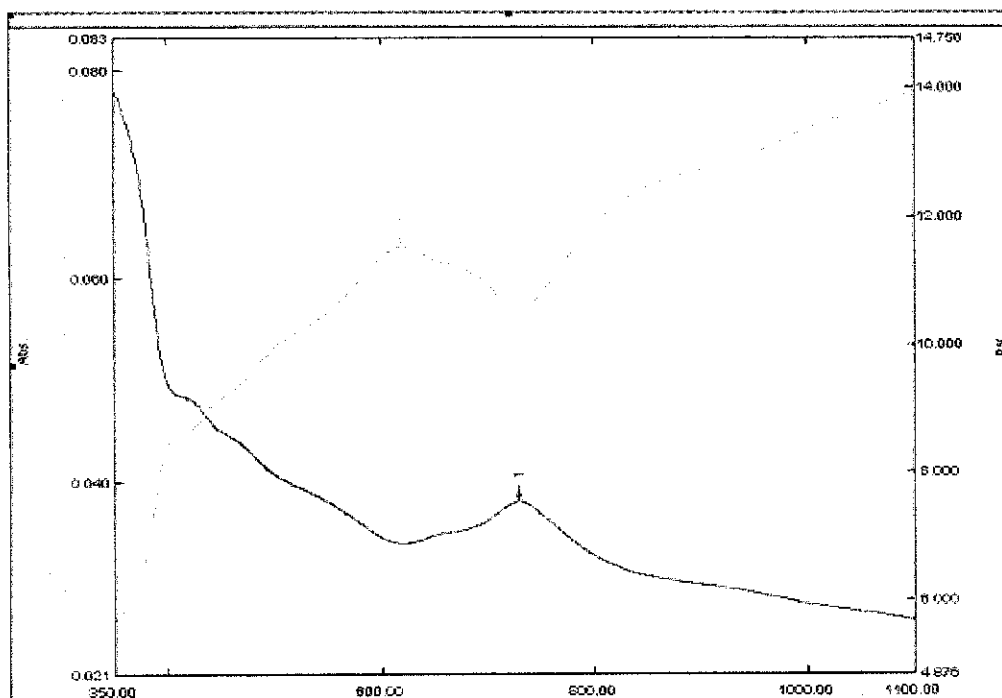


Fig 4.45 0.5 mol zinc chloride with 0.2 mol nickel(ii)nitrate (400 °C)

at 500 °C

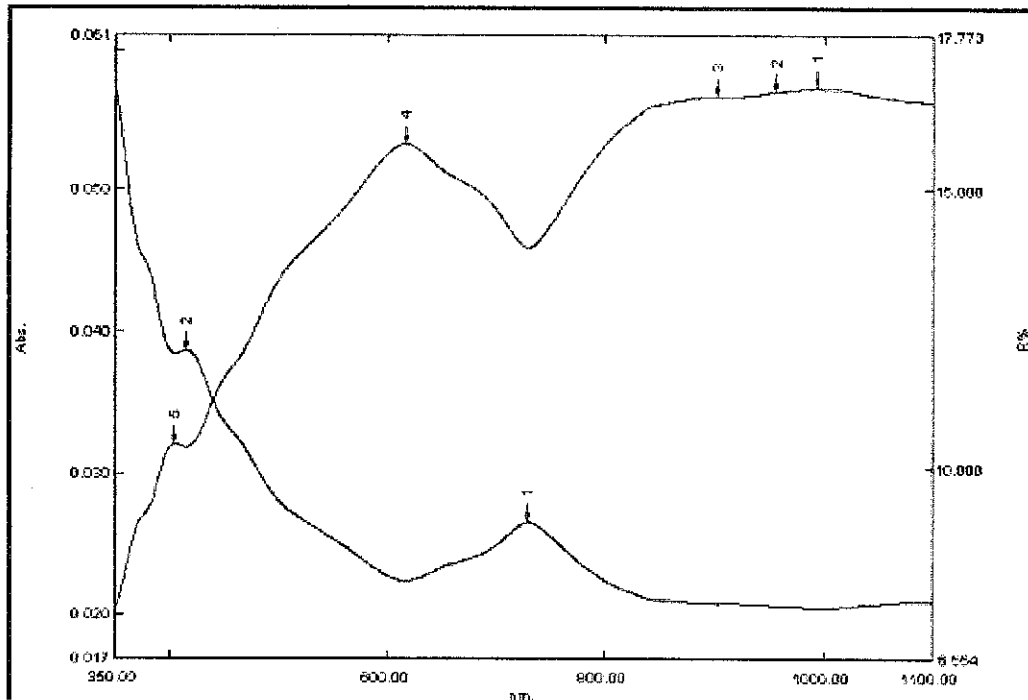


Fig 4.46 0.5 mol zinc chloride with 0.2 mol nickel(ii)nitrate (500 °C)

at 600 °C

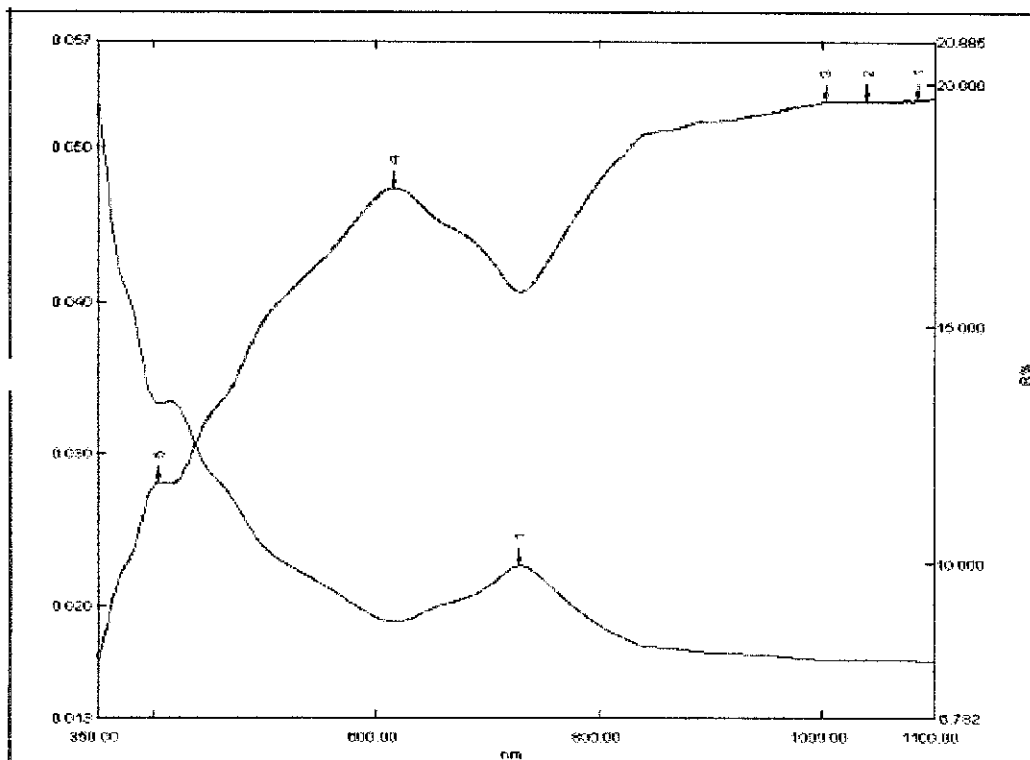


Fig 4.47 0.5 mol zinc chloride with 0.2 mol nickel(ii)nitrate (600 °C)

### Experiment 3

0.7 mol zinc chloride with 0.2 mol nickel(ii)nitrate

at 400°C

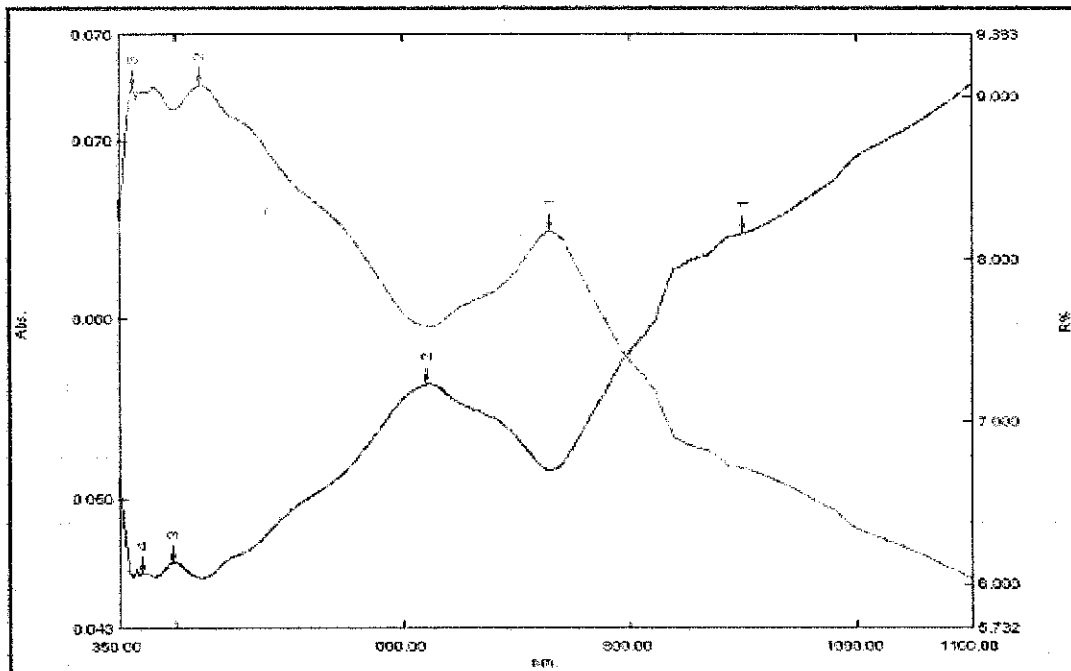


Fig 4.48 0.7 mol zinc chloride with 0.2 mol nickel(ii)nitrate (400 °C)

at 500 °C

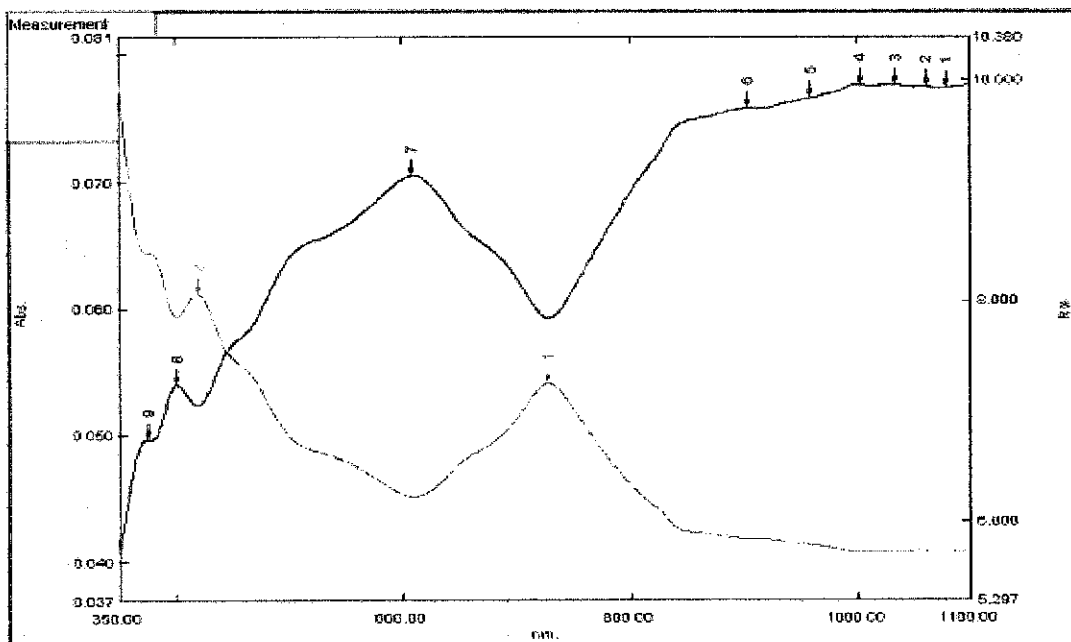
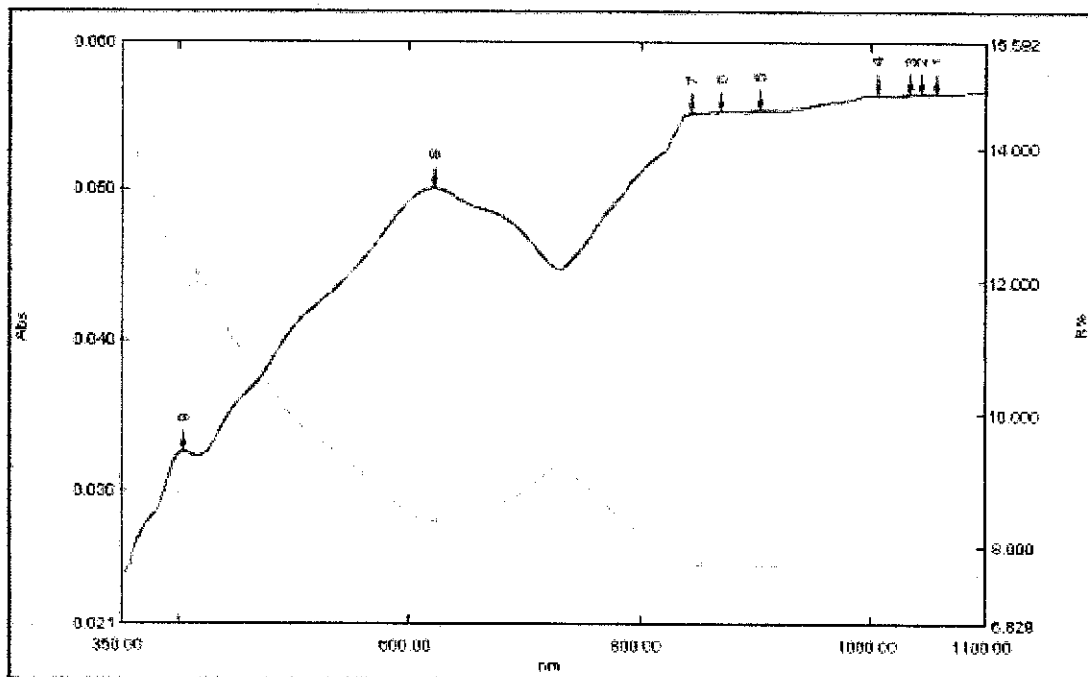


Fig 4.49 0.7 mol zinc chloride with 0.2 mol nickel(ii)nitrate (500 °C)



at 600 °C



**Fig 4.50** 0.7 mol zinc chloride with 0.2 mol nickel(ii)nitrate (600 °C)

#### **Experiment 4**

Approximately 0.5 mol of Zinc Chloride

at 400 °C

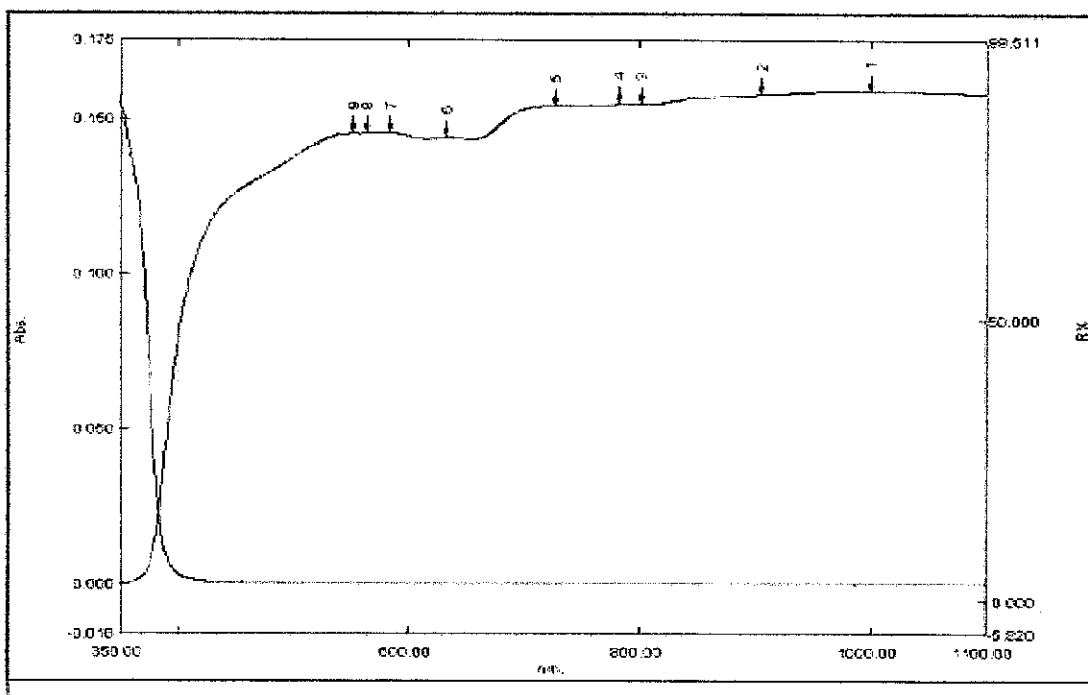


**Fig 4.51** Approximately 0.5 mol of Zinc Chloride (400 °C)

At 500°C

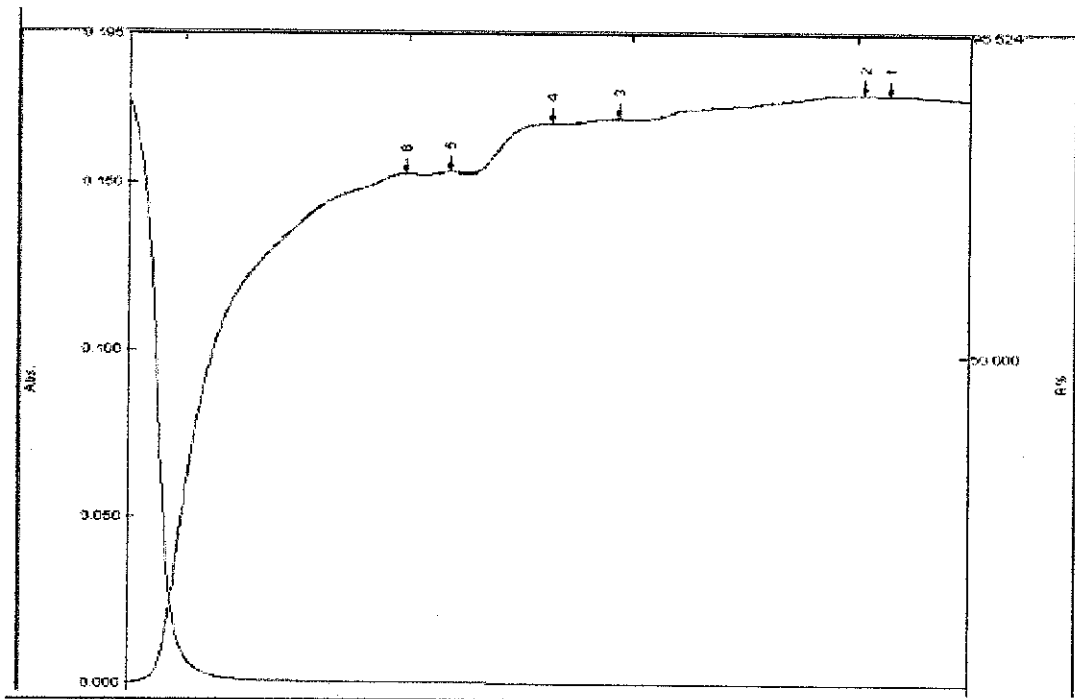


Fig 4.52 Approximately 0.5 mol of Zinc Chloride (500°C)

At 600°C

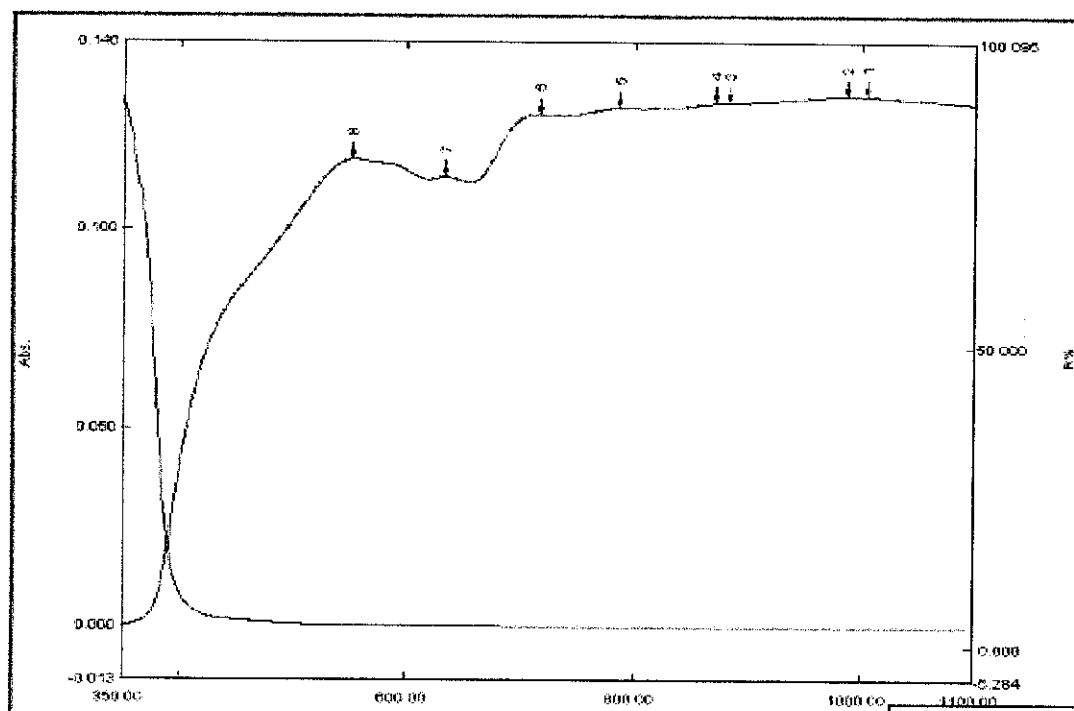


Fig 4.53 Approximately 0.5 mol of Zinc Chloride (600°C)

## **4.3 Discussion**

### **Physical Properties**

Based on the observation done, it is clear that different ratio of chemical used affects the concentration of refluxed mixture produced and the colour of samples for the calcinated samples. The higher portion of chemical used in the distribution of ratio to used will favor and influence the colour of samples refluxed. For example, the sample using 0.2 mol Zinc Chloride and 0.7 mol Nickel(ii)Nitrate will produce a sample that is more to green colour than the sample using 0.5 mol Zinc Chloride and 0.2 mol Nickel(ii)Nitrate. This observation is due to the fact that Nickel(ii)Nitrate exists as green solid in nature, while Zinc Chloride white in color. Therefore the green colour will favor more on the result. The same situation apply when changing sample having higher portion of Zinc Chloride.

The higher the ratio and volume of chemical used, the more concentrated the solution will be. For the samples of that has been treated in the furnace, it can be observed that higher calcinations temperature will result in finer and darker sample. This can be observed by comparing the result of using 400 °C ,500 °C and 600 °C. This observation is in agreement with findings from S. Aksoy et al, which stated that higher calcinations temperature will deteriorate the crystal structure and become amorphous.

### **Uv-Vis Result**

It can clearly be seen from the Uv-Vis graph, in desired range of visible light which is 320-750 nm, that higher temperature results in lower absorbance of  $ZiO-NiO$  nanoparticles and Zinc Oxide alone. This can justified by the studied conducted by Soumitra Kar that higher temperature results in smaller particles, smaller the particles, the larger the surface area, the greater the solar absorption [46]. As the temperature rises, the faster reaction rate and the increasing of supersaturation of reaction products lead to crystal core forming rate was accelerated in the short reaction time, that means the controlling step of the reaction is transferred from grain growth to crystal nucleus formation. With the temperatures continuing to rise, the phenomenon of "nuclear-aggregation" caused by the rapid formation of crystal nucleus is obvious that result in forming aggregate among the crystal nucleus so the particles are bigger which results

in lower surface area [44]. It can also be seen that the best concentration of ZnO is 0.5 mol and the best ratio is 2: 1 of ZnO to NiO by referring to the study conducted by FanZhang [6]. The concentration of reaction has a great effect on products' diameter. If too little of concentration being used, the solution is more difficult to reach the supersaturation than that in higher precursor concentration. Thus, submicron or soft agglomerates are easier to obtain rather than nanoparticles. If too high concentration being used therefore will result in more agglomeration that will reduce the surface area. With the increase of the supersaturation of the solution in response to the increasing of ion concentration in system, a great deal of crystal nuclei are generated instant of the reaction, which lead to tiny crystalline grains increased. So the "the size fraction agglomeration" phenomenon becomes gradually significant, and that result in the larger particles [47]. It can also be proven that by adding NiO to the ZnO nanoparticles will result in higher absorbance by comparing the graph of Zinc Oxide alone and graph of Zinc Oxide with Nickel (ii) Oxide. Defects and impurities on the graph which shows rocky part and not smooth curve refer to intrinsic types that include oxygen vacancies, zinc vacancies, zinc interstitials, oxygen interstitials and antisites species; these intrinsic defects tend to accumulate on the free surfaces (and internal interfaces) of ZnO particles thereby determine the surface states that are known to be electrically and chemically active [44].

## **CHAPTER 5**

### **CONCLUSION AND RECOMMENDATION**

All the experiment samples have not being tested yet with X-RD and SEM due to time constraint and also the long queue for the testing .However, 4 samples until the calcinations process step was done. Preliminary observations towards these samples are comparable with information obtained from literature reviews. It is expected that the results from three testing methods will show similar pattern with literature reviews as well and produce impressive and good quality of samples. The Uv-Vis results showed similar pattern with literature reviews except it has some impurities probably due to lab equipments defects. The graph shows a good correlation with the 3 variables being tested which are temperatures, ratios used, and addition of NiO to ZnO.

There are a few recommendations that can be implemented for future improvement in this project. Increase interest toward altered ZnO nanoparticles in variety of electric and electronic applications promise high commercial value for future related research. With sufficient time and improve management of laboratory's inventory, these following recommendations will surely enhance the effectiveness of the experiment:

1. Study the effect of different method used in producing ZnO nanoparticle with addition of other nanoparticle towards the semiconducting efficiency of ZnO nanoparticles.
2. Study the effect of duration time of calcinations process towards the electrical properties of ZnO nanoparticles with addition with other nanoparticle
3. Study the effect of different nanomaterials used to be paired with ZnO towards its electrical properties
4. Improve the laboratory equipments facilities and management.

## REFERENCES

1. Hernandezbattez, A (2008). "CuO, ZrO<sub>2</sub> and ZnO nanoparticles as antiwear additive in oil lubricants".
2. Nav Bharat Metallic Oxide Industries Pvt. Limited. Applications of ZnO. Access date January 25, 2009
3. Greenwood, Norman N.; Earnshaw, A. (1984), *Chemistry of the Elements*, Oxford: Pergamon, pp. 1336–37, ISBN 0-08-022057-6
4. Greenwood, Norman N.; Earnshaw, A. (1984), *Chemistry of the Elements*, Oxford: Pergamon, pp. 1336–37, ISBN 0-08-022057-6
5. Schumacher, Kai (Hofheim, DE) (2002) Titanium Oxide coated with Silicon
6. Fan Zhang & Jun Ling Yang (2009) Preparation of Nano-ZiO and its application
7. Shahrom B Mahmud, Synthesis and characterization of ZnO nanostructures.
8. Irish, D. E. (1963). "Raman Study of Zinc Chloride Solutions". *The Journal of Chemical Physics* 39: 3436
9. Yamaguchi, Toshio (1989). "X-ray diffraction and Raman studies of zinc(II) chloride hydrate melts, ZnCl<sub>2</sub>.rH<sub>2</sub>O (r = 1.8, 2.5, 3.0, 4.0, and 6.2)". *The Journal of Physical Chemistry* 93: 2620
10. Egon Wiberg, Arnold Frederick Holleman (2001) *Inorganic Chemistry*, Elsevier ISBN 0123526515
11. Greenwood, Norman N.; Earnshaw, A. (1997), *Chemistry of the Elements* (2nd ed.), Oxford: Butterworth-Heinemann, ISBN 0-7506-3365-4
12. J. M. Spero, B. Devito, L. Theodore "Regulatory chemical handbook" CRC Press, 2000, ISBN 0824703901, 9780824703905
13. Nicholson, J. W (1998). "The chemistry of cements formed between zinc oxide and aqueous zinc chloride". *Journal of Materials Science* 33: 2251
14. Jack L. Ferracane (2001). *Materials in Dentistry: Principles and Applications*. Lippincott Williams & Wilkins. ISBN 0781727332.
15. Setting reaction and resultant structure of zinc phosphate cement in various orthophosphoric acid cement-forming liquids, Park C.-K., Silsbee M. R., Roy D. M., *Cement and concrete research*, (1998), 28, 1, 141-150
16. Greenwood, N. N.; & Earnshaw, A. (1997). *Chemistry of the Elements* (2nd Edn.), Oxford: Butterworth-Heinemann. ISBN 0-7506-3365-4.
17. . International Occupational Safety and Health Information Centre (CIS) Access date January 25, 2009
18. Zinc oxide MSDS. Access date January 25, 2009.
19. Özgür, Ü. (2005). "A comprehensive review of ZnO materials and devices". *Journal of Applied Physics* 98: 041301
20. F. Porter "Zinc Handbook: Properties, Processing, and Use in Design" (CRC Press) 1991 ISBN 0824783409, 9780824783402
21. Look, D.C.; Hemsley, J.W.; Szelove, J.R. (1999). "Residual Native Shallow Donor in ZnO". *Physical Review Letters* 82 (12): 2552. doi:10.1103/PhysRevLett.82.2552.
22. Janotti, A.; Van De Walle, C.G. (2007). "Hydrogen multicentre bonds". *Nat Mater* 6 (1): 44. doi:10.1038/nmat1795

23. Kato, H (2002). "Growth and characterization of Ga-doped ZnO layers on a-plane sapphire substrates grown by molecular beam epitaxy". *Journal of Crystal Growth* 237-239: 538. doi:10.1016/S0022-0248(01)01972-8
24. Ohgaki, Takeshi (2008). "Positive Hall coefficients obtained from contact misplacement on evident n-type ZnO films and crystals". *Journal of Materials Research* 23: 2293. doi:10.1557/JMR.2008.0300
25. Ryu, Y. R. (2003). "Properties of arsenic-doped p-type ZnO grown by hybrid beam deposition". *Applied Physics Letters* 83: 87. doi:10.1063/1.1590423
26. D. Schulz *et al.* (2008). "Inductively heated Bridgman method for the growth of zinc oxide single crystals". *Journal of Crystal Growth* 310: 1832. doi:10.1016/j.jcrysgro.2007.11.050
27. Baruah, Sunandan (2008). "Growth of ZnO nanowires on nonwoven polyethylene fibers" (free download pdf). *Science and Technology of Advanced Materials* 9: 025009. doi:10.1088/1468-6996/9/2/025009
28. Miao, L. (2007). "Synthesis, microstructure and photoluminescence of well-aligned ZnO nanorods on Si substrate" (free download pdf). *Science and Technology of Advanced Materials* 8: 443. doi:10.1016/j.stam.2007.02.012
29. Nav Bharat Metallic Oxide Industries Pvt. Limited. Applications of ZnO. Access date January 25, 2009.
30. "zinc." Encyclopædia Britannica. 2009 Encyclopædia Britannica Online. 10 March 2009
31. Greenwood, Norman N.; Earnshaw, A. (1984), *Chemistry of the Elements*, Oxford: Pergamon, pp. 1336–37, ISBN 0-08-022057-6
32. General Information of Zinc from the National Institute of Health, WHO, and International Zinc Association accessed 10 March 2009
33. Zinc white accessed 10 March 2009
34. . "Database of Select Committee on GRAS Substances (SCOGS) Reviews". <http://www.accessdata.fda.gov/scripts/fcn/fcnDetailNavigation.cfm?rpt=scogsListing&id=372>. Retrieved 2009-08-03
35. Theodore Gray. The Safety of Zinc Casting Access date January 25, 2009
36. . J. B. Calvert. Zinc and Cadmium Last modified August 20, 2007. Access date January 25, 2009
37. Physico-chemical characterization and photocatalytic activity of zinc oxide prepared by various methods.K.M. Parida \*, S.S. Dash, D.P. Das.19 january 2009
38. K. Lascelles, L. G. Morgan, D. Nicholls, D. Beyersmann "Nickel Compounds" in Ullmann's Encyclopedia of Industrial Chemistry 2005 Wiley-VCH, Weinheim, 2005
39. "Handbook of Inorganic Chemicals", Pradniak, Pradyot; McGraw-Hill Publications,2002
40. "Toxicology and Carcinogenesis Studies of Nickel Oxide", U.S. Dept. of Health and Human Services, No. 451, 07/1996
41. Synthesis of nickel oxide nanoparticles using nickel acetate and poly(vinyl acetate) precursor N. Dharmaraj a,b,\*, P. Prabu c, S. Nagarajan d, C.H. Kimb, J.H. Park b, H.Y. Kimb,\* 18 Nov 2005.

42. Kister, Henry Z. (1992). *Distillation Design* (1st Edition ed.). McGraw-Hill. ISBN 0070349096.
43. , Robert H. and Green, Don W. (1984). *Perry's Chemical Engineers' Handbook* (6th Edition ed.). McGraw-Hill. ISBN 0070494797
44. Synthesis and characterization of ZnO nanostructures. Shahrom Bin Mahmud
45. Influence of Drying on the Characteristics of Zinc Oxide Nanoparticle C.P. Rezende<sup>1</sup>, J.B. da Silva<sup>1;2</sup>, N.D.S. Mohallem<sup>1</sup> | Laborat'orio de Materiais Nanoestruturados, Departamento de Qu'ımica, ICEx UFMG and <sup>2</sup>Centro de Desenvolvimento da Tecnologia Nuclear – CDTN/CNEN 31270-901 Belo Horizonte-MG, Brazil (Received on 1 July, 2008)
46. One-Dimensional ZnO Nanostructure Arrays: Synthesis and Characterization Soumitra Kar, Bhoja Nath Pal,<sup>‡</sup> Subhadra Chaudhuri,<sup>\*</sup> and Dipankar Chakravorty DST Unit on Nano Science & Department of Materials Science and DST Unit on Nano Science & ML Professor's Unit, Indian Association for the Cultivation of Science, Kolkata 700 032, India Received: November 18, 2005; In Final Form: January 13, 2006
47. Nickel and nickel oxide nanoparticles prepared from nickel nitrate hexahydrate by a low pressure spray pyrolysis. Wei-Ning Wang, Yoshifumi Itoh, I. Wuled Lenggoro, Kikuo Okuyama\* (January 2004)